Comptes Rendus

Géoscience

Sciences de la Planète

Charles Le Losq, Bjorn O. Mysen and George D. Cody

Water solution mechanism in calcium aluminosilicate glasses and melts: insights from *in* and *ex situ* Raman and ^{29}Si NMR spectroscopy

Glass, an ubiquitous material / *Le verre, un matériau omniprésent*

Water solution mechanism in calcium aluminosilicate glasses and melts: insights from *in* and *ex situ* Raman and ^{29}Si NMR spectroscopy

Charles Le Losq [*, a, b], **Bjorn O. Mysen** [b] **and George D. Cody** [b]

[a] Université Paris Cité, Institut de physique du globe de Paris, CNRS, F-75005 Paris, France

[b] Earth Planets Laboratory, Carnegie Institution for Science, Washington D.C. 20015, USA

E-mails: lelosq@ipgp.fr (C. Le Losq), bmysen@carnegiescience.edu (B. O. Mysen), gcody@carnegiescience.edu (G. D. Cody)

Abstract. New Raman and NMR spectroscopy data on hydrous Ca aluminosilicate melts and glasses, with eutectic quartz–anorthite–wollastonite composition, are presented here. The glasses were obtained by rapid quench of melts equilibrated at high P and high T in a piston–cylinder apparatus. *In situ* Raman observations of the structure of the melts were also performed during hydrothermal diamond cell experiments. Using the intensities of the ~860 cm^{-1} and ~1630 cm^{-1} Raman signals, respectively assigned to vibrations of T–OH and H$_2$O$_{mol}$ species, we determined the speciation of water in the glasses. T–OH and H$_2$O$_{mol}$ values compare well with those determined from infrared (IR) spectra, except above ~5 wt% total water where IR determinations actually underestimate the proportion of hydroxyl groups. The analysis of the polarized Raman spectra and of the ^{29}Si MAS NMR spectra of the hydrous glasses suggests limited changes in glass polymerization with variations in dissolved water content. However, at high temperatures, *in situ* Raman spectroscopy observations indicate that the hydrous melt structure differs very strongly from that of a glass containing a comparable concentration of dissolved water. Because of this, this study reinforces the fact that using glass data to try understanding high temperature processes in hydrous melts, like viscous flow or water diffusion toward bubbles during volcanic degassing, may not be very appropriate.

Keywords. Melt, Glass, Structure, Water, Speciation, Raman, NMR.

Published online: 6 May 2022, Issue date: 1 December 2022

1. Introduction

Water dissolved in magmas has been a longstanding topic of interest because of its critical influence on their properties, including viscosity [e.g., Leonteva, 1940, Saucier, 1952, Friedman et al., 1963, Dingwell et al., 1996, Richet et al., 1996], density [e.g., Ochs and Lange, 1999, Richet et al., 2000, Malfait et al., 2014a,b] and melting phase relations [e.g., Kushiro et al., 1968b,a]. In volcanic systems, water is recognized as being the engine of many types of volcanic eruptions [e.g., Gonnermann, 2015]. Such influence also extends back in time, such as for the formation of the first continents [Campbell and Tay-

---

* Corresponding author.

lor, 1983]. These observations have led to a number of experimental studies on the behavior of H_2O in melts to be undertaken using many different spectroscopic and/or modeling methods [e.g., Burnham, 1975, Stolen and Walrafen, 1976, Stolper, 1982, McMillan et al., 1986, Mysen and Virgo, 1986a,b, Farnan et al., 1987, Silver et al., 1990, Behrens et al., 1996, Davis and Tomozawa, 1996, Holtz et al., 1996, Mysen and Wheeler, 2000, Behrens et al., 2001, Xue and Kanzaki, 2004, 2006, Cody et al., 2005, Mysen and Cody, 2005, Behrens and Yamashita, 2008, Yamashita et al., 2008, Xue, 2009, Bouyer et al., 2010, Malfait and Xue, 2010, Malfait, 2014, Mysen, 2014, Chertkova and Yamashita, 2015, Le Losq et al., 2015c, 2017, Balzer et al., 2020, Cody et al., 2020].

Most of the existing data were obtained from the study of glasses quenched from melts equilibrated at high temperature and high pressure. In such glasses, water is supposed to be in a structural state representative of that in the melt at the glass transition, as suggested by infrared (IR) spectroscopy studies [e.g., Nowak and Behrens, 1995]. Few studies report *in situ* observations of the effect of water on the structure of alkali aluminosilicate melts at high pressure and high temperature [e.g., Mysen, 2009, 2010, 2014, Mysen and Yamashita, 2010, Chertkova and Yamashita, 2015]. The latter studies used hydrothermal diamond anvil cells [HDAC, Bassett et al., 1994, 1996] to perform optical as well as Raman/IR spectroscopy observations of melts and fluids at high temperature and high pressure. Except for the mentioned alkali aluminosilicate compositions, there is a general lack of *in situ* spectroscopic data for a broad range of melt compositions. This situation is unfortunate because (i) while water speciation derived from IR spectroscopy analysis appears frozen-in at the glass transition, the environment of H may change between high temperature (HT)–high pressure (HP) conditions and room T–room P (RT–RP) conditions, even in the glassy state; and (ii) the case of alkaline-earth compositions, very important for the magmatism of accretion and subduction zones, has been largely overlooked. Regarding (i), Le Losq et al. [2017] recently reported that the Raman O–H stretching signals of hydrous sodium silicate and aluminosilicate glasses appears very different if observed at room temperature or at 500 °C and ~200–500 MPa. This followed older reports of changes of the proton environment in glasses be-

tween the glass transition temperature and room temperature [Holtz et al., 1996, Le Losq et al., 2013], which result from large changes in hydrogen bonding in undercooled melts and glasses. Regarding (ii), the high liquidus of alkaline-earth aluminosilicate compositions results in difficult experimental conditions, explaining the lack of *in situ* studies focused on such compositions. As a result, there is currently a clear lack of integrated *in* and *ex situ* study of alkaline-earth aluminosilicate melts.

To help tackle this problem and provide new data pertinent for calc-alkaline and tholeiitic compositions important for the volcanism at accretion and subduction zones, we present here new *in* and *ex situ* data on melts and glasses of the ambient pressure eutectic quartz–anorthite–wollastonite composition. This composition in molten form has a degree of polymerization similar to typical andesite magmas (Number of Non-Bridging Oxygens per Tetrahedra, NBO/T = 0.41). *In situ* Raman spectroscopy data were acquired with the Ca aluminosilicate melt equilibrated with aqueous fluids in a HDAC. The high frequency part (OH stretching signals) of the Raman spectra acquired during those HDAC experiments were already reported in a previous publication [Le Losq et al., 2017]. Here, we focus on the interpretation of the low frequency part of the Raman data, where the signature of the silicate network is observed. To help this analysis, we studied through polarized Raman spectroscopy, the structure of hydrous Ca aluminosilicate glasses, quenched from melts equilibrated at high pressure and high temperature in a piston–cylinder apparatus. To help our interpretation of the HDAC Raman spectroscopy data, we also determined the water solubility in the Ca aluminosilicate melt up to 2 GPa, extending the original P–T space covered by the study of McMillan et al. [1986]. The new data stress that, at conditions representative of those of the Earth's interior, the structure of hydrous magmas is far from that usually inferred from glass data.

2. Methods

2.1. *Material synthesis*

Two batches of anhydrous Ca aluminosilicate (CA2 and CA3) glasses with a quartz–anorthite–wollastonite composition (64.84 mol% SiO_2,

9.06 mol% Al_2O_3, 26.11 mol% CaO, NBO/T = 0.41) were synthesized from dried reagent-grade $CaCO_3$, Al_2O_3 and SiO_2 powders. The powders were crushed for 1 h in a mechanical agate mortar, and placed in a Pt crucible. The starting materials were heated at a rate of 1 °C·min^{-1} in order to ensure a slow decarbonation process, to finally reach a temperature of 1400 °C. The melts were quenched into glass in air. After the initial melting, the glasses were crushed for 1 h in an agate mortar, and re-fused at 1400 °C. This was repeated three times, in order to ensure homogeneous glass starting materials. Analysis of the chemical composition of the glasses was performed through energy-dispersive X-ray spectrometry (EDS), with using a JEOL field-emission scanning electron microprobe (FE-SEM) equipped with an Oxford silicon drift detector. A 15 kV accelerating voltage and a 1.00 nA current were used. Measurements were performed scanning 25 by 25 µm areas. The EDS results were calibrated using the following standards: cossyrite for Na, pyrope for O and Si, ENAL20 for Al, and diopside for Ca. Calibration was based on a set of glass standards. The EDS results are within error of standards analyzed as unknowns (see Table 1).

2.2. *Hydrous glasses synthesis*

Hydrous glasses were obtained by hydration of melts at HT and HP in a piston–cylinder apparatus [Boyd and England, 1960]. Powder of the starting glass was placed in Pt capsules with the appropriate amount of water. The exact amount of added water was determined by weighing the capsules. For glasses with a low water concentration (<10 wt%), we used ~10 mm long by 5 mm diameter capsules. For glasses with $[H_2O] > 10$ wt%, aimed at testing the water solubility in the Ca aluminosilicate composition (see Section 2.8), small capsules of ~8 mm long by 3 mm diameter were used. Around 160 mg of hydrous glass can be produced with using the large capsules, whereas the small ones allow retrieving ~30 mg of glass. Using small capsules ensures a higher quenching rate, which avoids crystallisation of fluid-saturated melt and limits the formation of quench bubbles upon quench. The loaded and sealed capsules were placed in 3/4 inch diameter furnace assemblies based on the design of Kushiro [1976], and subjected to the desired pressure and temperature (see Tables 2 and 3) for 120 min in a

piston–cylinder. Temperatures were measured with type S thermocouples with no correction for pressure on their *emf*, which may be as much as 10 °C [Mao et al., 1971]. Pressure was calibrated against the melting point of NaCl and the calcite-aragonite transformation [Bohlen, 1984]. Estimated uncertainties are ~10 °C and ~0.1 GPa, respectively.

2.3. *Infrared spectroscopy*

Transmission infrared spectra of the hydrous glasses were recorded using a Jasco® IMV-4000 multichannel infrared spectrometer with a 10× objective, an MCT detector and the standard light source, a 100 µm aperture, and 1000 acquisitions. The glasses were double-polished to a thickness in the 50–200 µm range by using oil in order to avoid any reaction of their surfaces with water. The glass samples were placed on BaF_2 windows during measurements. After collection of each spectrum, the sample was moved aside and a background spectrum was recorded at the same spot. Division of sample spectra by background spectra gave the final absorbance spectra, which were normalized to samples thicknesses.

2.4. *Raman spectroscopy*

Raman spectra of various materials were recorded using two systems. Unpolarized Raman spectra of glasses and melts/fluids during *in situ* experiments were recorded at the Earth Planets laboratory using a Jasco NRS 3100 spectrometer, equipped with holographic gratings, a single monochromator, and a 1024 × 128 Andor DV401-F1 CCD Peltier-cooled detector operating at −70 °C. A 490 nm line of a Coherent solid state laser was used for sample excitation, with a power of ~33 mW on samples. The laser was focused on samples through a 50× Olympus lens. The Raman spectra of the glasses were recorded using a groove-density of the gratings of 2400 lines/mm, which results in an accuracy better than 3 cm^{-1} and a precision better than 1 cm^{-1}. During hydrothermal diamond anvil cell experiments, the Raman spectra of the different melts, fluid and crystal phases were recorded with using a groove-density of the gratings of 1200 lines/mm. The Raman spectra of the ^{13}C diamonds together with a Ne

Table 1. Chemical composition of anhydrous glasses

		SiO_2	Al_2O_3	CaO	NBO/T
Nominal values	Nom. mol%	64.84	9.06	26.11	0.41
	Nom. wt%	62.00	14.70	23.30	
Batch CA2	Meas. wt%	61.9(4)	14.7(1)	23.4(1)	
Batch CA3	Meas. wt%	62.2(4)	14.7(1)	23.1(2)	

Nom. mol%, Nom. wt% and Meas. wt% refer respectively to the nominal compositions in mol and wt%, and to the measured composition in wt%. Errors are given at the 1σ confidence interval in brackets; values and associated errors were rounded to the first significant digit.

Table 2. Water concentration in wt% and relative density of hydrous CA2 and CA3 glasses

Glass	Nom. $[H_2O^{TOT}]$	T–P	$[OH]^{IR}$	$[H_2O_{mol}]^{IR}$	$[H_2O^{TOT}]^{IR}$	$[H_2O^{TOT}]^{Raman}$	Relative density
CA3-DR	0.00		—	—	—	—	2.68(4)
CA2-1	1.00		0.96(6)	0.12(2)	1.08(7)	1.14(5)	*n.m.*
CA2-2	2.00		1.3(1)	0.55(9)	1.8(2)	2.1(1)	2.67(3)
CA3-3-1	3.00		2.1(1)	1.09(5)	3.2(1)	3.1(1)	2.60(6)
		1500 °C					
CA2-4	4.00		2.4(20)	1.8(20)	4.2(3)	3.8(1)	2.61(3)
		1.5 GPa					
CA3-6-1	6.00		2.5(1)	3.6(2)	6.1(2)	5.9(1)	2.49(4)
CA2-8	8.00		2.6(2)	5.4(4)	8.0(4)	7.9(1)	2.47(2)
CA2-9.5	9.5		—	—	—	9.7(1)	—

CA3-DR is an anhydrous densified glass that was prepared in the piston–cylinder, so that its density is comparable to other hydrous glasses prepared at the same pressure. Nom. $[H_2O^{TOT}]$ refers to the nominal total water concentrations. ^{IR} and ^{Raman}: measurements made with using Infrared and Raman spectroscopy, respectively. Errors are given at the 1σ confidence interval in brackets; values and associated errors were rounded to the first significant digit.

Table 3. Water solubility in the CAS melts

Pressure (MPa)	Temperature (°C)	Water content (wt%)
1000	1000	11.0(2)
1000	1100	10.8(6)
1000	1200	11.4(5)
1100	1200	14.1(5)
1200	1200	15.6(9)

Errors are given at the 1σ confidence interval in brackets; values and associated errors were rounded to the first significant digit.

reference line, used for pressure estimates, were acquired with using a 532 nm laser line, and a 2400 grooves/mm grating to ensure the best Raman shift accuracy. Alignment of the Raman spectrometer was tested against the 520.7 cm^{-1} Raman peak of pure Si.

Polarised Raman spectra of the glasses were recorded at IPGP using a Horiba HR Evolution Raman spectrometer. This spectrometer is equipped with a single monochromator, and a Symphony OE Peltier-cooled detector operating at −60 °C. A 487.77 nm line of a Coherent solid state laser was used for sample excitation, with a power of ~25 mW on samples. The laser was focused on samples through a 100× Olympus lens. The Raman spectra of the glasses were recorded using a groove-density of the gratings of 1800 lines/mm and a confocal hole aperture set at 50, which results in an accuracy of ~1.2 cm^{-1} and a precision better than 1.0 cm^{-1}. Alignment of the Raman spectrometer was tested against the reference 546.07 nm line of room Neon lights as well as

the 520.7 cm^{-1} Raman peak of a monocrystalline Si wafer.

2.5. *Solid-state NMR spectroscopy*

^{29}Si solid-state NMR experiments were carried out with a Chemagnetics CMX Infinity 300 solid-state NMR spectrometer, with a magnetostatic field strength of ~7.05 T. This implies a ^{29}Si Larmor frequency of 59.6 MHz. ^{29}Si Magic Angle Spinning (MAS) NMR spectra were acquired by spinning the samples at 4 kHz. ^{29}Si excitation pulse widths of 1.3 µs were performed at a 30° tip angle, with a pulse delay of 200 s. The spectral width was of 20 kHz. The number of acquisitions was 400, requiring 1 day per sample.

2.6. *Density measurements*

The density of the hydrous glasses (Table 2) was measured with using the Archimedes method, by immersion in toluene. The weights of dry and immersed glass pieces were measured using a Berman balance at the Earth Planets laboratory. From these measurements, it is possible to calculate the density of the glass pieces because the toluene density and its variations with temperature are precisely known. This method has an accuracy of 0.001 [e.g., Richet et al., 2000]. In the present case, the available Berman system resulted in a larger error, equal to 0.04. The obtained values are in good agreement with those reported by Silver et al. [1990] for the same composition.

2.7. *Water concentration and speciation in hydrous Ca aluminosilicate glasses*

The 4500 and 5200 cm^{-1} IR absorption bands, respectively assigned to combination modes of vibrations from OH groups and H_2O_{mol} species [Stolper, 1982], were used to determine the concentration and speciation of water in the hydrous CA2 and CA3 glasses (Table 2). A 6th order polynomial function was used to subtract the background below the IR absorption bands. The concentration of OH groups and H_2O_{mol} species were obtained with using the absorption coefficients from Silver et al. [1990].

2.8. *Solubility measurements*

Solubility measurements for the present eutectic Ca aluminosilicate composition have been reported by McMillan et al. [1986] and Silver et al. [1990]. However, at temperatures below 1200 °C (the limit of the hydrothermal diamond anvil cell setup), only solubility measurements up to 500 MPa have been reported [McMillan et al., 1986]. To address this issue, phase equilibria and Raman spectroscopy measurements were used to determine the solubility of water in the Ca aluminosilicate melt above 1 GPa at 1200 °C. The H_2O solubility in the melt at any temperature and pressure is defined by the univariant equilibrium melt ↔ melt + fluid [Burnham and Jahns, 1962, Mysen and Acton, 1999]. Experiments with different amounts of water were performed at given T and P, embracing the univariant equilibrium. Experiments in which the melts were saturated with water, fluid vesicles were observed, allowing us to estimate the location of the univariant equilibrium boundary. Uncertainties affecting the phase equilibria method range between 0.5 to 2%, depending on the spacing of the different experiments that were performed. An independent confirmation was obtained through Raman spectroscopy. This was possible because the high (~1 µm) spatial resolution of Raman spectroscopy allows avoiding fluid vesicles and quench bubbles, and, hence, observing only O–H stretching signals from water dissolved in the glasses. A calibration relating the total glass water content to the ratio of the Raman signals assigned to O–H stretching vibration and silicate vibration in the glass [see Le Losq et al., 2012, and references cited therein] was established with using the CA2 and CA3 glasses with 1 to 8 wt% water as standards (Table 2). The Raman spectra were treated following the protocol described in Le Losq et al. [2012], using the r*ameau()* function implemented in the *rampy* Python library [Le Losq, 2018].

2.9. *Hydrothermal diamond anvil cell (HDAC) experiments*

Results of the *in situ* experiments carried out in an externally heated HDAC [Bassett et al., 1994, 1996] with 1 mm diamond cutlets were reported in Le Losq et al. [2017]. Chips of the glasses and ^{13}C diamond were loaded together with distilled water into the sample chamber. A "double gasket" setup, with outer Re

and inner Pt rings, was used as it does not deform at temperatures above 800 °C. The experimental chamber was of ~300 μm diameter by ~100 μm height. The temperature in the HDAC was controlled to within 1 °C with chromel–alumel thermocouples that were in contact with the surface of the upper and lower diamond anvils. The accuracy of the temperature measurements is better than 3 °C [Bassett et al., 2000]. The pressure inside the cell is governed by the PVT relationship of the pressure-generating aqueous fluid: at fixed volume, increasing temperature results in increasing pressure. Pressure was estimated by using the pressure-/temperature-dependent one-phonon Raman shift of the synthetic ^{13}C diamond. This shift has been calibrated in the 0.1–1500 MPa and 25–800 °C ranges by Mysen and Yamashita [2010]. The Ne emission lines, recorded together with the Raman spectra of the ^{13}C diamond, were used as references to determine the exact Raman shift of the ^{13}C diamond Raman peak, which results in a ±0.1 cm^{-1} uncertainty. This frequency uncertainty results in pressure precision of ±40 MPa. By taking the uncertainty in the calibration of the Raman shift into consideration, total pressure uncertainty in the experiments was ±110 MPa.

The pressure and temperature conditions, the visual observations as well as the 2700–4000 cm^{-1} portion of Raman spectra are provided in Le Losq et al. [2017]. Here, we focused on treating the 600–1300 cm^{-1} portion of Raman spectra acquired during those experiments. In this frequency range, the Raman spectra are affected by the nearby presence of the strong ~1332 cm^{-1} diamond signal from the anvils. To remove its effect on the spectra, we acquired a Raman spectrum of the diamond anvil, pointing the laser on the gasket without changing its optical focus, right after the acquisition of a sample Raman spectrum. The 1220–1270 and 1340–2499 cm^{-1} portions of the Raman spectra, where no signal from the sample is expected, were used to adjust the signal intensity from the Diamond spectrum to that of the diamond signal in the Sample spectrum, following a protocol similar to the one performed for removing the 2nd order Diamond signals from the D–O stretching signals in Dalou et al. [2015a]. A least square routine corrects the Diamond and Sample spectra from any shift in frequency and then adjusts the diamond signal from the Diamond spectrum to that in the Sample spectrum. Then, the

adjusted diamond signal is removed from the Sample spectrum. This results in a diamond-corrected sample Raman spectrum in the 600–1250 cm^{-1} Raman shift range. After this treatment, the Raman signals were corrected from temperature and excitation line effects [see Le Losq et al., 2012, and references reported therein], using the *tlcorrection()* function implemented in the *rampy* library. The intensity in the corrected spectra has been normalized to the total integrated intensity measured between 600 and 1250 cm^{-1} by trapezoidal integration.

3. Results

3.1. *Raman spectra of glasses*

Polarized, raw Raman spectra of the hydrous glasses are shown in Figure 1. In the 0–2000 cm^{-1} portion of the spectra, broad bands centered near 80 cm^{-1}, 500 cm^{-1} and 1050 cm^{-1} are visible. The 80 cm^{-1} band is called the Boson peak, and is a low frequency vibrational signature of amorphous materials. Its origin remains controversial. It is a localized vibration that can be assigned to collective transverse acoustic vibrational modes [Shintani and Tanaka, 2008], which in silicate glasses are promoted by cooperative inter-tetrahedral librations [Bucheneau et al., 1986, Chumakov et al., 2011]. Its intensity is sensitive to the glass fictive temperature [Malinovsky and Sokolov, 1986], while its frequency is affected by the mean atomic volume [Nakamura et al., 2013]. Here, the Boson peak intensity (BPI) increases by a factor 2 with increasing the glass water content from 0 to 9.5 wt% (Figure 2a). This reflects the effect of the expected decrease in glass transition temperature with water addition [see Deubener et al., 2003, and references cited therein]. In parallel, the Boson peak frequency (BPF) decreases slightly (by 6 cm^{-1}). Such change is more difficult to interpret, and remains in any case small.

A strong, polarized band near ~500 cm^{-1} is observed (Figure 1). Its intensity is not affected by glass water content. Small shoulders near 575 and 650 cm^{-1} are also present. The intensity of those contributions depends on the water content of the glasses. All those signals arise from the bending/breathing modes of Si–O–Si bonds that link Q^n units [e.g., see Bell et al., 1968, Sen and Thorpe, 1977, Furukawa and White, 1980, Furukawa et al.,
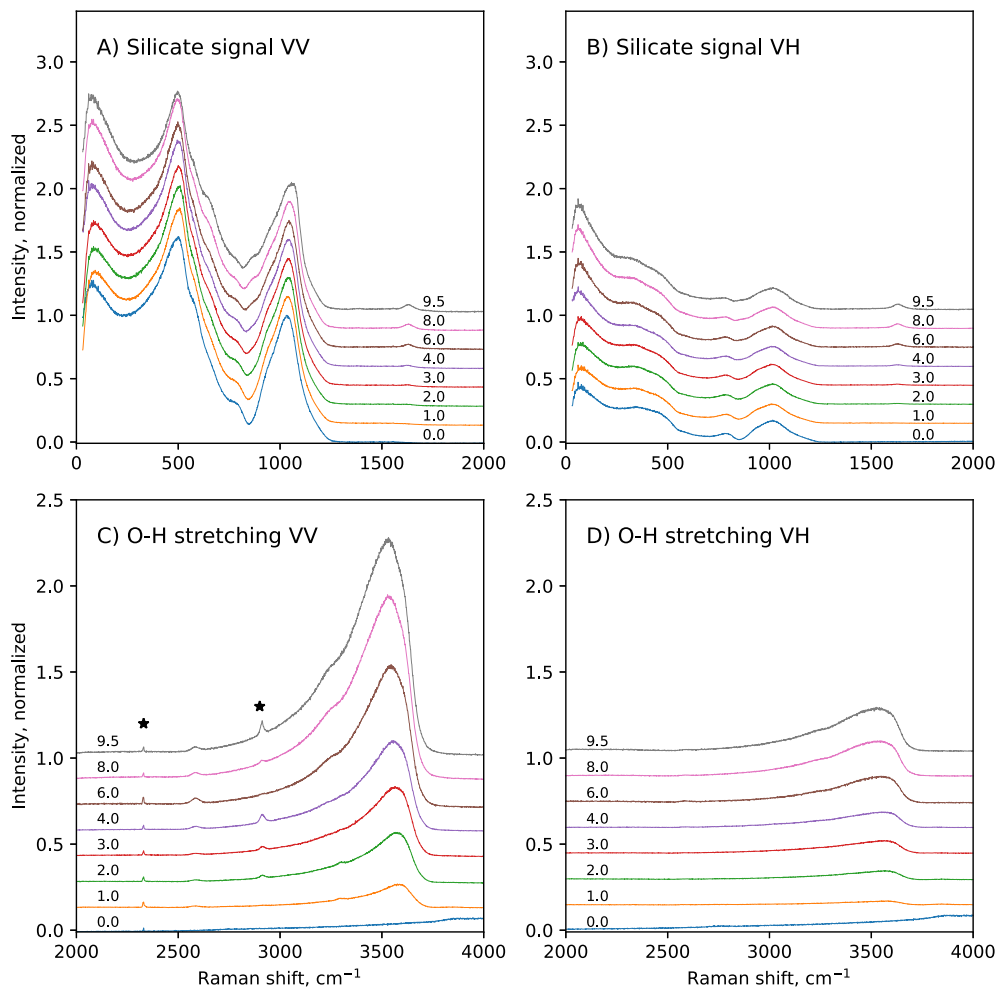
Figure 1. Polarized Raman spectra of the hydrous CAS glasses. The numbers indicate the nominal water content of the glasses in wt%. The sharp peaks indicated by stars are signals from surface impurities or atmosphere. Intensity was normalized to the maximum of the 800–1300 cm^{-1} band observed on VV spectra.

1981, McMillan, 1984]. From the model of Furukawa et al. [1981], the main 500 cm^{-1} band may be assigned to T–O–T vibrations involving Q^3 and Q^4 units (Q^n designates a tetrahedral cation [Si,Al] in fourfold coordination surrounded by n bridging oxygens, and carrying 4-n non-bridging oxygens). The 575 cm^{-1} shoulder can be assigned to T–O–T vibrations involving Q^2 units. The origin of the 650 cm^{-1} peak is more difficult to decipher and probably involves complex Q^n–Q^n vibrations, probably with $n = 2$ or 3 given that the present glasses have NBO/T values lower than 1 (see discussion).

A shoulder near 795 cm^{-1} is visible in the VV spec-

tra (Figure 1A). It actually is a depolarized band, visible in the VH spectra at ~785 cm^{-1} (Figure 1B). Observed in the VH spectra, this band is asymmetric and presents a shoulder near ~815 cm^{-1}, and the band intensity decreases with increasing the glass water content. In the VV spectra, the ~795 cm^{-1} shoulder disappears with increasing the glass water content. This signal may be assigned to vibrations involving the motion of Si in its oxygen cage [McMillan, 1984], possibly related to the threefold—degenerate "rigid cage" vibrational mode of SiO_2 tetrahedra [Sen and Thorpe, 1977, Galeener, 1979]. Another possible attribution would be Si–O stretching in Q^0 units [Mysen
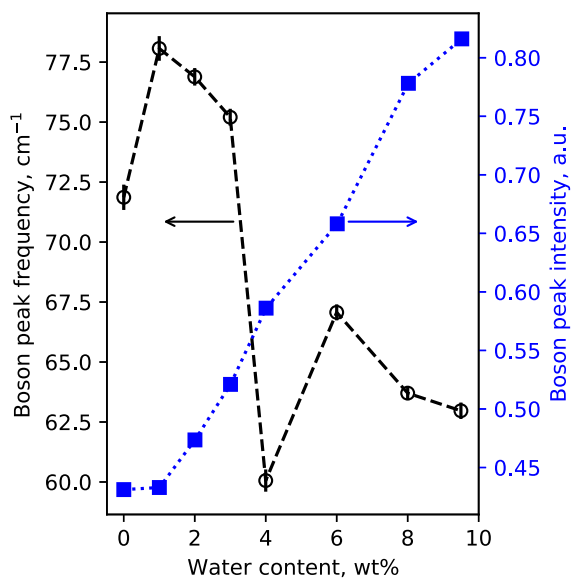
Figure 2. Boson Peak Intensity (BPI, filled blue squares) and Boson Peak Frequency (BPF, open black circles) measured on the VH spectra presented in Figure 1. BPI and BPF were determined from the fit of the 0–130 cm^{-1} portion of VH spectra with a log normal function; in this restrained frequency range, the Boson peak maximum is well fitted by such a function. Lines are guides for the eyes.

et al., 1982, McMillan, 1984], but here the NBO/T of the hydrous glass always remain below 1, so Q^0 units with a NBO/T of 4 are not expected to be present.

In the 800–1300 cm^{-1} portion of spectra, a broad band is observed (Figure 1A,B). In the VV spectra, its maximum is located near 1040 cm^{-1}, a shoulder near 941 cm^{-1} is visible, and another one near 860 cm^{-1} grows with increasing the glass water content (Figure 3A). A slope break is also visible on the high frequency side of this band, near 1180 cm^{-1}. The position of the maximum in the VV spectra slightly shifts to higher frequencies with increasing glass water content: it is at ~1032 cm^{-1} in the anhydrous CA glass, and at ~1058 cm^{-1} in the glass with 9.5 wt% water. In the VH spectra, the ~860 cm^{-1} and ~940 cm^{-1} shoulders are also visible, but with much lower intensities (Figure 3B). The slope break near 1180 cm^{-1} is also visible. The maximum of the broad band is not at ~1040 cm^{-1} anymore, but is located at ~1014 cm^{-1}. This position remains con-

stant regardless of the glass water content. According to literature [e.g., Brawer and White, 1975, 1977, Furukawa and White, 1980, Mysen et al., 1982, McMillan, 1984, Neuville, 2006, Malfait, 2009a,b, Le Losq et al., 2015c], the 860 cm^{-1} signal can be assigned to vibrations from T–OH groups (T = Si, Al), the 940 cm^{-1} shoulder to Si–O stretching in Q^2 units, and the 1040–1050 cm^{-1} band to Si–O stretching in Q^3 units. The high frequency shoulder near 1180 cm^{-1} can be assigned to T–O stretching in Q^4 units (T = Si, Al). The shift in frequency of the intensity maximum of the 800–1300 cm^{-1} spectral envelop from ~1040–1060 cm^{-1} in the VV spectra down to 1014 cm^{-1} in the VH spectra indicates that the Q^3 unit signal is highly polarized, and that a less polarized signal exists near 1000–1020 cm^{-1}. The latter probably is the signal reported by various authors in peak fitting models of spectra of aluminosilicate glasses, assigned to (i) Si–BO stretching [Mysen et al., 1982], (ii) asymmetric stretching of Q^n units [Spiekermann et al., 2012, Le Losq et al., 2014] or (iii) additional Q^3 signals [You et al., 2005, Nesbitt et al., 2019]. The hypothesis (iii) is difficult to reconcile with the fact that the 1040–1060 cm^{-1} band is more polarized that the signal near 1014 cm^{-1}. Indeed, as the depolarization ratio depends on the symmetry of the vibration (the higher it is, the lower the ratio), it should be quite constant for a given vibrational mode like the symmetric T–O vibration in Q^3 units. Furthermore, the hypothesis (iii) does not agree with studies using linear decompositions of Raman spectra [Zakaznova-Herzog et al., 2007, Malfait, 2009a, Herzog and Zakaznova-Herzog, 2011] as well as molecular dynamics [Zotov et al., 1999, Spiekermann et al., 2012, 2013], which point to the existence of additional vibrational contributions from all Q^n units in the 1000–1060 cm^{-1} frequency range. This is corroborated by the analysis of Raman spectra of fully polymerized silica and tectosilicate glasses, all showing a peak in the 1000–1060 cm^{-1} frequency range [Seifert et al., 1982, Neuville and Mysen, 1996, Le Losq and Neuville, 2013, Le Losq et al., 2014, Novikov et al., 2017]. Given the existing vibrational and simulation data on silica and aluminosilicate glasses, the most plausible hypothesis for the origin of the signal near 1014 cm^{-1} in the present glasses is T–O asymmetric stretching in Q^n units (T_{2s} vibrational mode) [see discussion in Le Losq and Neuville, 2013, Le Losq et al., 2014, and references therein].
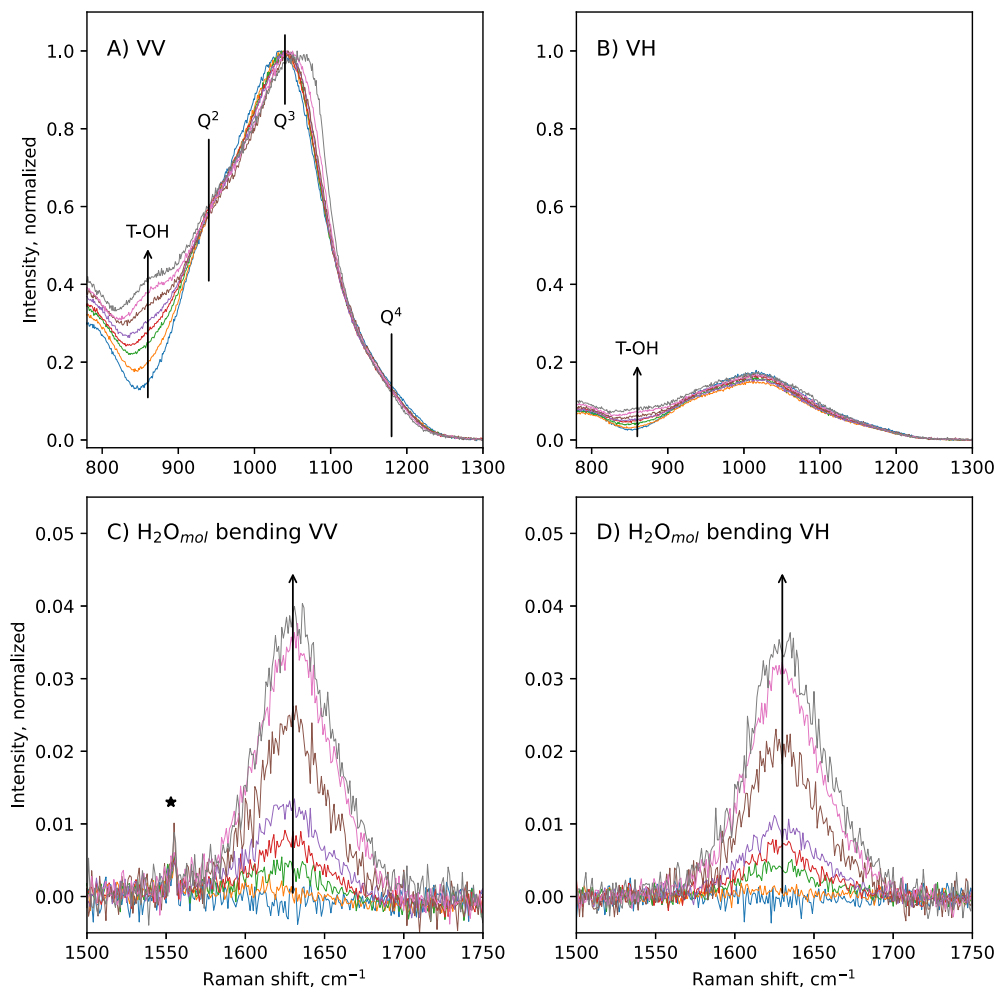
Figure 3. Zoom on the 800–1300 cm^{-1} and the 1500–1750 cm^{-1} portions of VV (A, C) and VH (B, D) Raman spectra of the hydrous CAS glasses. Signals assigned to T–OH vibrations (with T = Si, Al) as well as T–O vibrations in Q^2, Q^3 and Q^4 units are materialized by vertical lines in (A). The ~1630 cm^{-1} peak assigned to H$_2$O$_{mol}$ bending, which grows with glass water content, is clearly visible in the spectra (arrow in C, D). The sharp peaks indicated by stars are signals from surface impurities or atmosphere.

Above 1300 cm^{-1}, a sharp band at ~1630 cm^{-1} appears in hydrous glasses (Figures 1, 3). Its intensity increases with increasing glass water content. This band is depolarized: the depolarization ratio VH/VV is nearly equal to 1 (Figure 3C,D). As asymmetric molecules tend to present depolarized signals, this indicates that the molecule and its vibration yielding this signal are asymmetric. This agrees with the assignment of this band to bending vibrations of water molecules [e.g., Walrafen, 1964]. This band can thus be assigned to vibrations from molecular water H$_2$O$_{mol}$ being dissolved in the glass.

In the 2000–4000 cm^{-1} portion of the Raman spectra, we observe that increasing the glass water content leads to the appearance and growth of a broad, asymmetric band with a maximum centered near 3550 cm^{-1} (Figure 1C,D). At high water content, shoulders at ~3240 cm^{-1} and ~3615 cm^{-1} are visible. The position of the maximum intensity of this broad band decreases with increasing the glass water content. In the VV spectra, it is at ~3581 cm^{-1} in the glass with 1.0 wt% H$_2$O, and ~3532 cm^{-1} in the glass with 9.5 wt% H$_2$O. This band can be assigned to O–H stretching from water species dissolved in the

glasses [Walrafen, 1964, 1975, Stolen and Walrafen, 1976, Walrafen and Samantha, 1978, McMillan and Remmele Jr, 1986, Mysen and Virgo, 1986a].

3.2. *Raman signals related to water species in the glasses*

In the above Raman spectra, three different signals are assigned to vibrations of water molecules (H_2O_{mol}) at ~1630 cm^{-1}, of T–OH hydroxyl groups at ~860 cm^{-1}, and of O–H stretching in water molecules and hydroxyl groups in the glasses at ~3580 cm^{-1}. The integrated intensity (a.k.a. area under the curve) of the later signal varies linearly with the nominal water content of the glasses (Figure 4A). This allows actually obtaining a linear calibration that links the water content of the glasses to the area under the 2500–4000 cm^{-1} O–H stretching band [Thomas, 2000, Behrens et al., 2006, Le Losq et al., 2012, Schiavi et al., 2018]. This calibration was used to determine the water content in water-saturated samples obtained during the solubility experiments (see Section 3.3).

The H_2O_{mol} 1630 cm^{-1} signal intensity varies nonlinearly with the glass water content (Figure 4B). The intensity shown in Figure 4B was actually measured on the VH spectra, because it is less affected by the surrounding background in VH spectra than in VV spectra (see Figure 3C,D). The H_2O_{mol} 1630 cm^{-1} signal VH intensity shows a concave upward variation with glass water content, indicating that more and more H_2O_{mol} species are present as glass water content increases. This observation differs from that on the 860 cm^{-1} shoulder assigned to T–OH. In Figure 4C, the relative intensity of this signal was measured at 860 cm^{-1} on the VV spectra by difference with that on the VV Raman spectrum of the anhydrous glass; this relative intensity shows a concave downward variation with glass water content.

From the variation of the Raman signals assigned to T–OH hydroxyl groups and water molecules, we propose a method to determine the water speciation from the VV and VH Raman spectra of glasses in which the M–OH content (with M a metal cation, like Ca) can be considered as negligible. Therefore, we assume that $c_{OH} \approx c_{T–OH}$, with c_{OH} and $c_{T–OH}$ the concentrations of total OH groups and T–OH groups, respectively. This assumption is reasonable in the present case because, given the NMR study of Xue and Kanzaki [2008] on diopside–anorthite glasses,
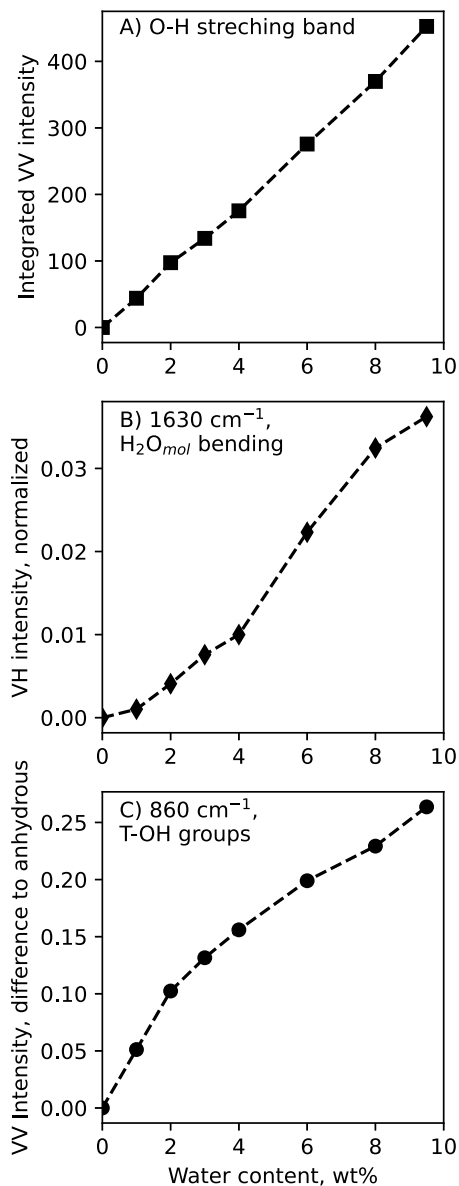

Figure 4. (A) Integrated intensity (a.k.a. area under the curve) below the ~3600 cm^{-1} O–H stretching band, measured on the VV spectra. (B) Intensity of the ~1630 cm^{-1} H_2O_{mol} bending band, measured on the VH spectra. (C) Intensity at 860 cm^{-1}, measured by difference to that in the anhydrous glass Raman spectrum. All VV and VH Raman intensities were normalized to the maximum intensity in the 800–1300 cm^{-1} portion of the VV Raman spectra prior to any calculation. Lines are guides for the eyes. Errors bar are smaller than symbol size.

we expect a maximum of 6% (relative to total H) of M–OH groups in CaO–MgO–Al$_2$O$_3$–SiO$_2$ glasses with anhydrous NBO/T lower than 0.5. As a first approximation, the fraction of M–OH groups can thus be considered as negligible in our glass composition, with an anhydrous NBO/T of 0.41. We thus have

$$c_{\text{water}} = c_{\text{OH}} + c_{\text{H}_2\text{O}_{\text{mol}}} = c_{\text{T–OH}} + c_{\text{H}_2\text{O}_{\text{mol}}}. \quad (1)$$

To determine $c_{\text{T–OH}}$ and $c_{\text{H}_2\text{O}_{\text{mol}}}$ from the Raman spectra, we need the Raman Cross Sections (RCS) of the T–OH groups and H$_2$O$_{\text{mol}}$ species. In particular, as the T–OH signals are better resolved on VV spectra while the H$_2$O$_{\text{mol}}$ signal is more resolved on VH Raman spectra, we need the RCS of those signals, respectively $\text{RCS}_{\text{T–OH}}^{\text{VV}}$ and $\text{RCS}_{\text{H}_2\text{O}_{\text{mol}}}^{\text{VH}}$. Knowledge of those values allows one to calculate the concentrations of T–OH groups and H$_2$O$_{\text{mol}}$ from the observed polarized Raman intensities at 860 and 1630 cm^{-1}, I_{860}^{VV} and I_{1630}^{VH}:

$$c_{\text{T–OH}} = \text{RCS}_{\text{T–OH}}^{\text{VV}} \times I_{860}^{\text{VV}}, \quad (2)$$

$$c_{\text{H}_2\text{O}_{\text{mol}}} = \text{RCS}_{\text{H}_2\text{O}_{\text{mol}}}^{\text{VH}} \times I_{1630}^{\text{VH}}. \quad (3)$$

Combining (2) and (3) with (1), it is possible to write:

$$\frac{\text{RCS}_{\text{T–OH}}^{\text{VV}} \times I_{860}^{\text{VV}}}{c_{\text{water}}} = 1 - \frac{\text{RCS}_{\text{H}_2\text{O}_{\text{mol}}}^{\text{VH}} \times I_{1630}^{\text{VH}}}{c_{\text{water}}}. \quad (4)$$

This should yield a straight line relationship in a $I_{860}^{\text{VV}}/c_{\text{water}}$ versus $I_{1630}^{\text{VH}}/c_{\text{water}}$, and the intersections with the abscissa and ordinate will allow calculating $\text{RCS}_{\text{H}_2\text{O}_{\text{mol}}}^{\text{VH}}$ and $\text{RCS}_{\text{T–OH}}^{\text{VV}}$.

Figure 5 shows the $I_{860}^{\text{VV}}/c_{\text{water}}$ versus $I_{1630}^{\text{VH}}/c_{\text{water}}$ plot for the present data. Prior to measurement, each VV and VH spectra were normalized to the VV integrated intensity measured between 800 and 1300 cm^{-1}. To only get signals from T–OH vibrations, I_{860}^{VV} was corrected from the intensity at 860 cm^{-1} in the Raman spectrum of the anhydrous glass. The correlation between $I_{860}^{\text{VV}}/c_{\text{water}}$ and $I_{1630}^{\text{VH}}/c_{\text{water}}$ is good and allows calculating $\text{RCS}_{\text{H}_2\text{O}}^{\text{VH}} = 0.0070 \pm 0.0007$ and $\text{RCS}_{\text{T–OH}}^{\text{VV}} = 0.063 \pm 0.004$.

Using (2) and (3), it is now possible to directly determine the water speciation from the Raman spectra (VV and VH) of the hydrous glasses. This only requires knowledge of the glass water content, which can be measured by Raman spectroscopy using the intensity of the broad O–H stretching band for instance (e.g., Figure 4A). Figure 6 shows the result of such a calculation. A good agreement between the Raman-determined and IR-determined OH and
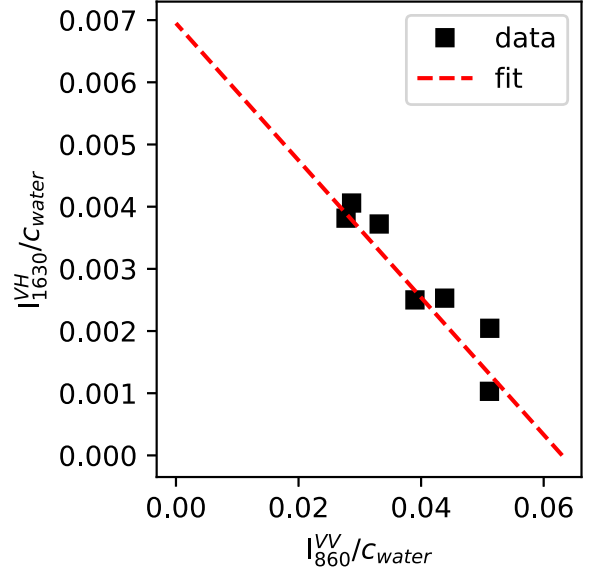

Figure 5. Relationship between $I_{860}^{\text{VV}}/c_{\text{water}}$ and $I_{1630}^{\text{VH}}/c_{\text{water}}$, as expected from (4). The intersections on this plot allows calculating the Raman cross sections of the OH and H$_2$O$_{\text{mol}}$ species (see text and (1) to (4)). Errors bar are smaller than symbol size.

H$_2$O$_{\text{mol}}$ species is observed up to $c_{\text{water}} = $ ~5 wt%. Raman spectroscopy returns c_{OH} values higher than IR spectroscopy, and $c_{\text{H}_2\text{O}_{\text{mol}}}$ values lower. Relative error bars affecting c_{OH} and $c_{\text{H}_2\text{O}_{\text{mol}}}$ determination by Raman spectroscopy are of ~6 and ~9%, respectively. They are similar to those affecting values determined from IR spectroscopy. Given those error bars, the disagreement between Raman-determined and IR-determined c_{OH} and $c_{\text{H}_2\text{O}_{\text{mol}}}$ values above $c_{\text{water}} = $ ~5 wt% is significant. Its origin will be discussed in Section 4.1.

3.3. Q^n speciation from Raman data

To extract information about glass polymerization in terms of Q^n units, it is possible to model the 800–1300 cm^{-1} portion of spectra with a sum of peaks assigned to (Si,Al)–O stretching signals in different Q^n units. However, in the present glasses, usual least-square methods tend to fail because of the important overlap of several contributions in a narrow spectral region. Indeed, from existing studies and the observation of spectra (see Section 3.1 and references
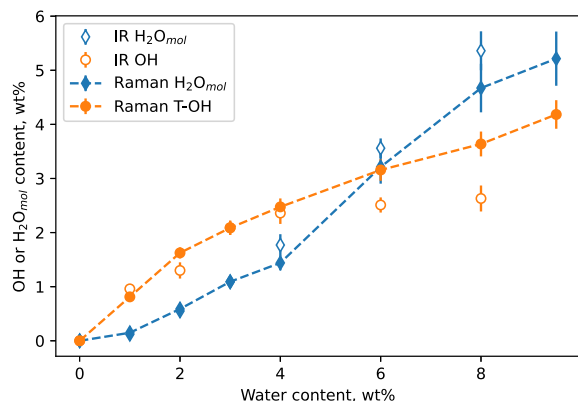
Figure 6. Concentration in OH and H_2O_{mol} species of the hydrous CAS glasses as a function of total water content, as measured independently by infrared IR spectroscopy (open diamonds) and Raman spectroscopy (closed diamonds). Lines are guides for the eyes. If not visible, errors bar are smaller than symbol size.

cited therein), we expect (i) a peak near 860 cm^{-1} assigned to OH group vibrations, (ii) a peak near 950 cm^{-1} assigned to T–O stretching in Q^2 units, (iii) a peak near 1000–1050 cm^{-1} assigned to asymmetric T–O stretching in Q^n units, (iv) a signal near 1050–1100 cm^{-1} assigned to T–O stretching in Q^3 units, and (v) one peak (or possibly two in highly polymerized glasses) between 1100 and 1250 cm^{-1} assigned to T–O stretching in Q^4 units. We do not expect to see strong signals from Q^0 or Q^1 units because, even considering the most hydrous glasses, the estimated NBO/T of the present glass series remains well below 1 (see below), and the main units at play should be the Q^2, Q^3 and Q^4 ones. Of course, this does not rule out the presence of those units because other factors like T or composition affect the $2Q^n = Q^{n-1} + Q^{n+1}$ equilibria, but there is no clear indication of their presence in the glass spectra. However, before going further, it is necessary to take into account the Al/Si ratio in the Q^n units, which causes the frequency of the bands to shift to lower values [Seifert et al., 1982, Neuville and Mysen, 1996, Neuville et al., 2004]. We do expect the peaks assigned to vibrations in Q^n units to be shifted to frequencies lower than those reported for Al-free silicate glasses, and this should be taken into account to initialize the peak-fitting models. The peak(s) assigned to Q^4 units should be more affected by this effect, because

Al preferentially substitutes Si in Q^4 units [Mysen et al., 2003], particularly in Ca-bearing compositions with more than 45 mol% SiO_2 as indicated by ^{27}Al MQ-MAS NMR data [Neuville et al., 2006]. Therefore, from existing data recording the effect of the Si/Al ratio on the frequency of Q^n units in CaO–Al$_2$O$_3$–SiO$_2$ glasses [Neuville et al., 2004, 2008], the Q^4 signal should be located near 1135 cm^{-1}, the Q^3 signal near 1050 cm^{-1}, and the T_{2S} signal near 1020 cm^{-1}. This expected position of the Q^3 signal agrees with the maxima observed in VV spectra, near 1050 cm^{-1}. Similarly, the expected position for the T_{2S} signal agrees with the maximum observed near ~1114 cm^{-1} in VH spectra. The frequency of the Q^2 signal is not expected to be significantly affected by the Al/Si substitution because ^{27}Al MQ-MAS NMR data indicate that Al is not present in Q^2 units in Ca aluminosilicate glasses with more than 45 mol% SiO_2 [Neuville et al., 2006]. This agrees with the position of the Q^2 shoulder near 950 cm^{-1} in the present VV and VH spectra, a frequency that agrees with previous literature reports [e.g., Furukawa et al., 1981, Mysen et al., 1982, Matson et al., 1983, McMillan, 1984].

Previous studies reported that the shape of peaks assigned to Q^n units is mostly Gaussian in aluminosilicate glasses [Mysen et al., 1982, Seifert et al., 1982, Neuville and Mysen, 1996, Le Losq et al., 2014]. Recent studies in Cs silicate glasses suggest peaks for Q^3 and Q^2 units with important Lorentzian contributions [Bancroft et al., 2018, Nesbitt et al., 2019]. However, other studies of the Raman spectra of Ca, Na and K silicate glasses also point to Gaussian peak shapes [e.g., Mysen, 1990, Zotov et al., 1998, Neuville, 2006, Le Losq et al., 2015c]. To check this for the present Ca aluminosilicate glasses, we tested models with Gaussian, Lorentzian and pseudo-Voigt peak shapes. The model with Lorentzian peaks did not converge. The model with pseudo-Voigt peaks converged but with very high Gaussian to Lorentzian ratios. The choice of Gaussian peaks thus is appropriate in the present case. In any case, the adopted peak shape is only an approximation, as the true shape of T–O stretching in Q^n units may be more complex, as shown by results from simulations [e.g., Zotov et al., 1999, Spiekermann et al., 2012, 2013] and linear spectral decomposition [Zakaznova-Herzog et al., 2007, Malfait, 2009a, Herzog and Zakaznova-Herzog, 2011]. From existing studies in Ca silicate compositions [e.g., Neuville, 2006], the half width at half maxi-

mum of the Gaussian peaks should be comprised between 25 and 35 cm^{-1}, approximately.

For peak fitting the spectra, we thus have information from previous studies. To use such pieces of information in the mathematical modeling of the spectra, a Bayesian approach is adopted. This approach differs from the traditional statistical peak-fitting methods in several ways: (i) first, we are not searching for the "best" model but we sample a range of plausible models given the data we have at hand, each model being associated with a probability; (ii) we can use the information we have from previous studies to guide the model sampling; (iii) given a sufficiently large set of sampled models, errors on the model parameters can be robustly evaluated without any assumption regarding their statistical distribution. All this relies on the use of the Bayes theorem, which states that the *log posterior probability* of a model is obtained from the sum of its *log likelihood* and its *log prior*. The *log likelihood* is the joint probability of the data given the model parameters. The *log prior* encodes the known information about the model. With expressions for those two terms, we can sample models that reconstruct the data given different sets of parameters, calculate their probabilities, and obtain a good picture of the models landscape.

To construct the *log likelihood* expression, we will compare how a model reconstructs both the VV and VH spectra simultaneously. The VV part of the model, G^{VV}, is thus a sum of k Gaussian peaks of amplitude a, Raman shifts ω^0, and half width at half maximum l:

$$G^{\mathrm{VV}} = \sum_{i=1}^{k} a_i \exp\left(-\log(2) \times \left(\frac{\omega - \omega_i^0}{l_i}\right)^2\right). \quad (5)$$

To obtain the VH part of the model, each peak is affected by its depolarization ratio coefficient dr:

$$G^{\mathrm{VH}} = \sum_{i=1}^{k} dr_i \times a_i \exp\left(-\log(2) \times \left(\frac{\omega - \omega_i^0}{l_i}\right)^2\right). \quad (6)$$

Given signals y_n^{VV} and y_n^{VH} affected by noise σ_n^{VV} and σ_n^{VH} sampled at Raman shifts ω_n, the *log likelihood* of a model is equal to:

$$\begin{aligned}
&\ln p(y^{\mathrm{VV}}, y^{\mathrm{VH}} | \omega, a, \omega^0, l, dr) \\
&= -\frac{1}{2} \sum_n \left[\left(\frac{(y_n^{\mathrm{VV}} - G_n^{\mathrm{VV}})}{\sigma_n^{\mathrm{VV}}}\right)^2 + \ln(2\pi\sigma_n^{\mathrm{VV}}\sigma_n^{\mathrm{VV}}) \right. \\
&\left. \quad + \left(\frac{(y_n^{\mathrm{VH}} - G_n^{\mathrm{VH}})}{\sigma_n^{\mathrm{VH}}}\right)^2 + \ln(2\pi\sigma_n^{\mathrm{VH}}\sigma_n^{\mathrm{VH}}) \right]. \quad (7)
\end{aligned}$$

Now that we have an expression for the *log likelihood*, we need an expression for the *log prior*. Here, we use four multivariate Gaussian distributions to encode the existing pieces of information about the positions ω^0, amplitude a, width l and depolarization ratio dr of the various peaks. For ω^0, we can use the previously estimated positions of the peaks as means of the *prior* distribution on ω^0, $\overline{\omega_{\mathrm{prior}}^0} = [780, 860, 940, 1014, 1051, 1135 \ \mathrm{cm}^{-1}]$. We also can use the observed spectral intensities at those positions as means of the *prior* distribution on a, $\overline{a_{\mathrm{prior}}} \sim [0.3, 0.05, 0.5, 0.2, 0.9, 0.2]$. For the *prior* distribution on l, means were selected given previous publications on similar glass compositions [e.g., Mysen et al., 1982, Seifert et al., 1982, Neuville, 2006] as $\overline{l_{\mathrm{prior}}} \sim [40, 30, 55, 40, 40, 60]$. Given the average depolarization ratio of the 800–1300 cm^{-1} portion of the Raman spectra, we also used $\overline{dr_{\mathrm{prior}}} = 0.2$ (all peaks) for the prior distributions on dr. The standard deviations of those prior distributions were adjusted depending on the estimated knowledge and model instability: we favored high standard deviations to avoid constraining too much the model, but a balance has to be found because too vague priors tend to result in convergence failure. Finally, the Gaussian prior distributions were truncated to exclude the negative domain, as all parameters should be real positive numbers. In practice, we calculated the *log prior* as the sum of the truncated Gaussian distributions of ω^0, a, l and dr.

With expressions for the *log likelihood* and the *log prior*, one can calculate the posterior probability of a model given the data. Now, our aim is to sample a subset of models representative of the model posterior probability distribution, and then to draw conclusions regarding our problem from the analysis of this sample of models. To perform the sampling step, the usual approach is to use random-walk algorithms, such as the Metropolis–Hasting algorithm. In this study, we used the No-U-TurnS (NUTS) sampler [Hoffman and Gelman, 2014] implemented in the Python PyMC3 library. This sampler is based on the Hamiltonian Monte Carlo (HMC) algorithm [Neal, 2011]. It samples the model space via a random walk guided by Hamiltonian dynamics, using the information from the gradients to ensuring a more efficient sampling strategy than a traditional random Metropolis–Hasting algorithm for instance. Compared to vanilla HMC, NUTS is an extension

with no hand-tuning at all, very easy to use with libraries such as PyMC3 [Salvatier et al., 2016]. After sampling one thousand models (initialization *advimap*, 200,000 init steps, 2000 tuning steps), statistics on the different model parameters were estimated; as their distributions followed a Gaussian statistics, we make use of the means and standard deviations in the following. All calculations performed with model parameters (e.g., for calculating peak areas, Q^n unit fractions, etc.) were done using the full sample of models, such that reported results following those calculations are the means values and standard deviations characterizing the distributions of calculated values.

Figure 7 shows a set of VV/VH spectra together with a random sub-sample of 100 possible models, for the anhydrous glass as well as for that with 6 wt% water. The VV and VH spectra are well reproduced. The models retrieve well all the peaks inferred from literature knowledge and the observation of the spectra. The joint VV/VH modeling strategy is thus very powerful. It leverages the information from both signals and allows further constraining peak parameters. The observed mean depolarization ratios are: 0.13 ± 0.04 for the ~860 cm^{-1} peak, 0.200 ± 0.009 for the ~950 cm^{-1} Q^2 peak, 0.20 ± 0.02 for the ~1014 cm^{-1} T_{2S} peak, 0.09 ± 0.01 for the ~1060 cm^{-1} Q^3 peak, and 0.21 ± 0.01 for the ~1120 cm^{-1} Q^4 peak. We note that the present modeling helps confirming the presence of the T_{2S} peak in the Raman spectra of aluminosilicate glasses. Indeed, for glasses with M/Al > 1 (with M an alkali or alkaline-earth cation), this peak usually does not appear clearly in unpolarized Raman spectra [e.g., see spectra in Mysen and Toplis, 2007, Le Losq et al., 2014, Dalou et al., 2015b, Bechgaard et al., 2017] or in VV spectra (Figure 3a). Here, the joint modeling of the VV and VH spectra clearly resolves the presence of this peak (Figure 7).

Using the sample of possible models, we can follow how the signals in the 800–1300 cm^{-1} portion of the Raman spectra change with the glass water content (Figure 8a). Changes are very limited. The main variation is that of the 860 cm^{-1} peak assigned to T–OH group vibrations, which increases in intensity with increasing glass water concentration. The parameters of the other peaks change only slightly with water content, inducing very little changes in the areas of the peaks assigned to Q^n units. This observation is surprising, given an expected change in

NBO/T (ΔNBO/T = NBO/T^{hyd} − NBO/T^{anh}) of ~0.28 with the addition of 9.5 wt% water, calculated from both Raman and infrared water speciation data under the assumption that all OH groups are bonded to tetrahedral cations. Using the areas of the Q^2 and Q^3 peaks and the relative method presented in Le Losq et al. [2015c], it is possible to calculate ΔNBO/T variations with glass water content (Figure 8b). Those are much too limited (grey squares in Figure 8b) compared to those estimated from the fractions of T–OH groups determined from Raman or IR spectroscopy (solid and open diamonds in Figure 8b, respectively).

3.4. ^{29}*Si SP MAS NMR spectra*

To try understanding the Raman observations, we acquired the ^{29}Si SP MAS NMR spectra of the glasses with 0, 3 and 6 wt% water. Very small, if not negligible differences are observed between the ^{29}Si SP MAS NMR spectra of those glasses (Figure 9), which mostly consist of a broad symmetric band centered near −105 ppm. More precisely, the chemical shift of the band is at ~−104.4 ppm in the anhydrous glass, and at ~−104.6 ppm in the glass with 6 wt% water. The width at half maximum of the spectra barely varies with water content. It is at ~11 ppm for all glasses. A change in Q^n speciation implies significant variations in the shape of the ^{29}Si NMR spectra, as observed when adding alkali into silica [e.g., Maekawa et al., 1991] or when adding water in silicate glasses [e.g., Cody et al., 2005, Le Losq et al., 2015c]. Here, within the resolution of the present 1D ^{29}Si NMR spectra, there is no significant changes (Figure 9), in agreement with the Raman results (Section 3.3 and Figure 8). Both datasets actually indicate that the Si speciation in Q^n units barely changes with water addition into the glasses, at least up to 6 wt%. We note that such result agrees with the ^{29}Si NMR data of Cody et al. [2020] on hydrous sodium aluminosilicate glasses with 0, 5, and 10 wt% H$_2$O, which showed only limited differences between the NMR spectra of the glasses with 0 and 5 wt% H$_2$O; larger differences were observed between the ^{29}Si NMR spectra of the glasses with 0 and 10 wt%.

3.5. *Water solubility*

Using the linear relationship observed in Figure 4A, it is possible to recover the glass water content from
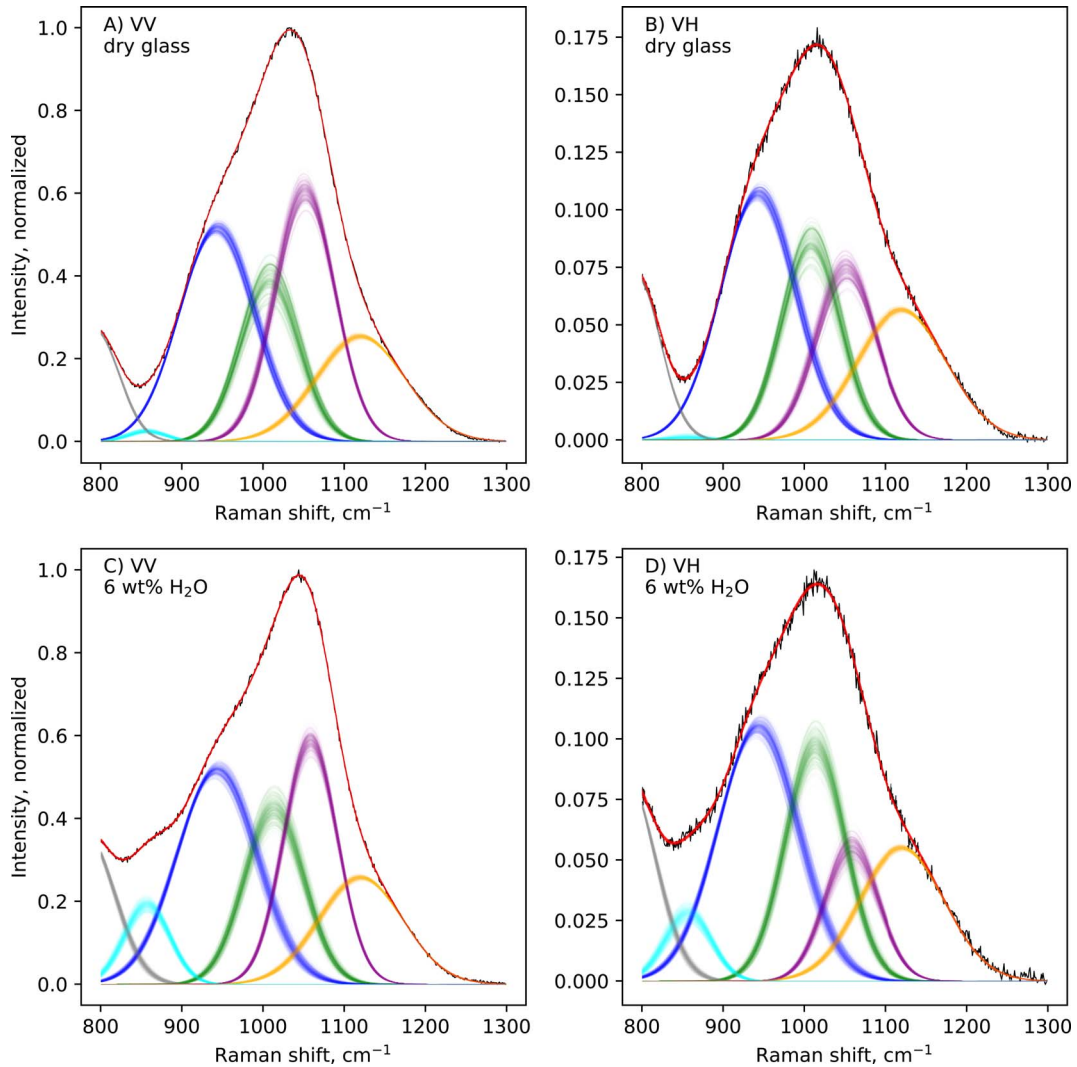
Figure 7. Example of Bayesian modeling of the 800–1300 cm^{-1} portion of the VV and VH Raman spectra (black lines) of a CAS glass with 6 wt% water. A subset of 100 posterior models, obtained by NUTS sampling (see text), are represented overlapping. The curves are affected by a transparency coefficients, so that a more intense color means a higher density of models, so a higher probability. For one model, the sum of its Gaussian components (grey, cyan, blue, green, purple and orange lines) yields the global model (red line).

its Raman spectra [e.g., see original publications of Thomas, 2000, Chabiron et al., 2004, Zajacz et al., 2005, Behrens et al., 2006, Di Muro et al., 2006]. Raman spectra thus allowed measurement of the glass water content in samples equilibrated in the piston–cylinder at high pressure and high temperature, under and over-saturated with water. For example, Figure 10A shows how the water content de-

termined from the Raman spectra of the samples changes as a function of the nominal water content in the Pt capsule, for a run at 1200 °C and 1.0 GPa. We observed that, below saturation, samples were bubble-free and Raman-determined water contents are close or below the nominal values. Above saturation, vesicles appear and Raman-determined water contents are systematically below the nominal
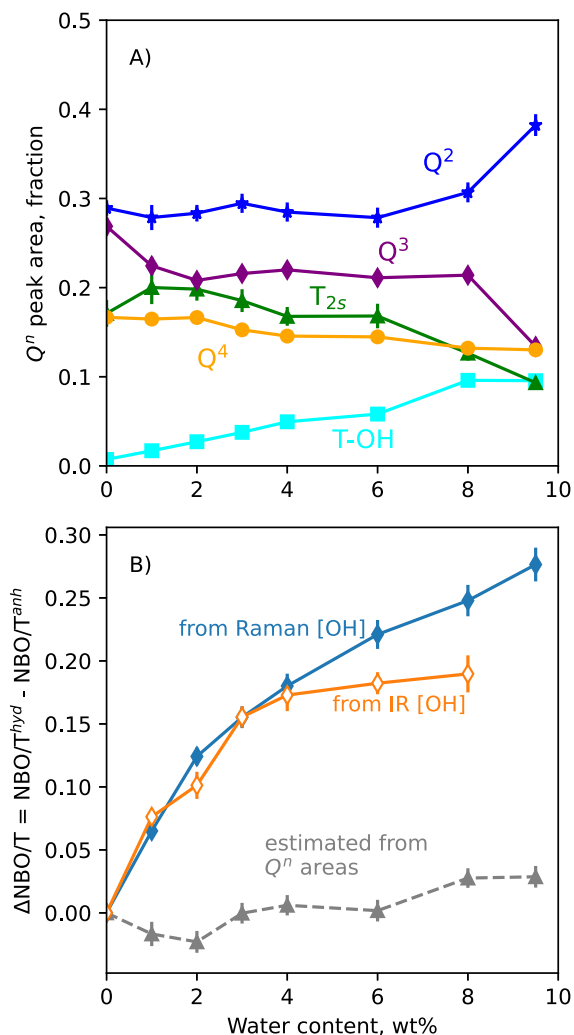
Figure 8. (A) Area of the Gaussian bands assigned to T–O stretching vibrations in Q^2 (blue stars), Q^3 (purple diamonds), and Q^4 units (orange circles), to T–OH group vibrations (cyan squares), and T_{2s} asymmetric stretching vibrations in Q^n units (green triangles). (B) Comparison between the change in glass NBO/T with water content calculated from IR (empty orange circles) and Raman (solid blue circles) water speciation data (Figure 6), assuming all OH groups interacting with Si or Al, or calculated from the variations in the peak areas (grey triangles). Lines are guides for the eyes. If not visible, errors bar are smaller than symbol size.

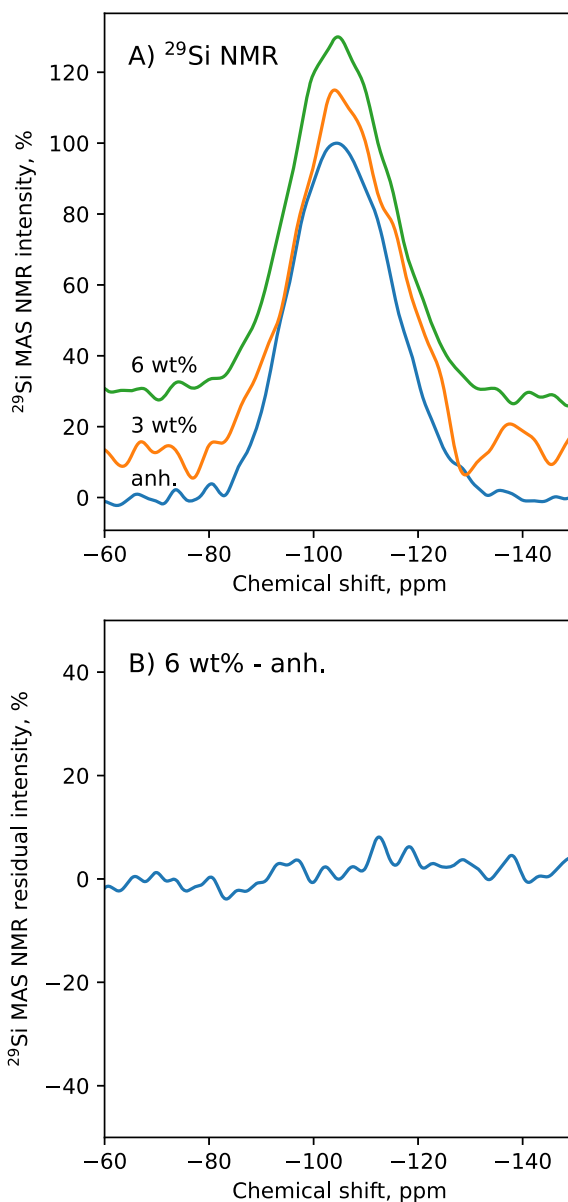values. In Figure 10A, glasses obtained from capsules with nominal water contents from 12 to 22 wt%

Figure 9. (A) ^{29}Si MAS NMR spectra of the glasses containing 0 wt% (anh.), 3 wt% and 6 wt% water. (B) difference between the ^{29}Si MAS NMR spectra of the anhydrous and 6 wt% water glasses.

present water contents ranging from 10.8 ± 0.2 wt% to 11.6 ± 0.7 wt% (standard deviations are calculated from the analysis of 5 to 10 Raman spectra). This yields a solubility limit at 11.4 ± 0.5 wt%.

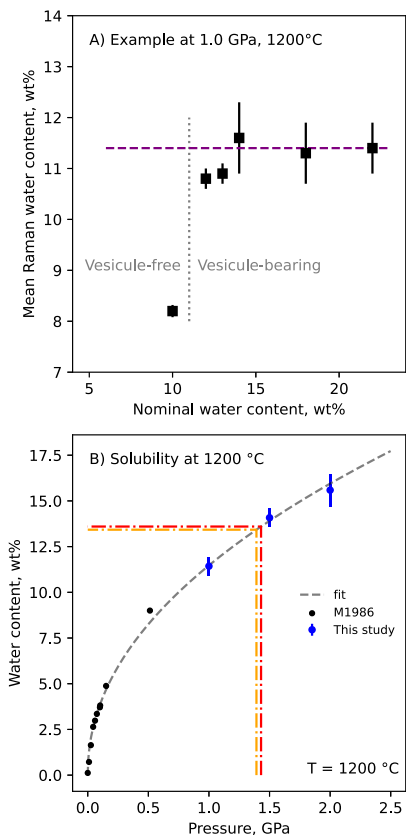Using the protocol described previously, we de-

Figure 10. Water solubility in the eutectic anorthite-quartz-wollastonite CAS glasses. (A) Example of the determination of the water content at saturation of a melt equilibrated with and without excess water at 1.0 GPa and 1200 °C. Below 11 wt%, no large vesicles are observed; above, large fluid vesicles are observed, and Raman-determined water contents all range around 11.4 ± 0.5 wt%. Each symbol is calculated from the mean of 5–10 different Raman measurements. (B) Water solubility at 1200 °C as a function of pressure. Data from McMillan et al. [1986], abbrev. M1986 in the caption, are also shown. Good agreement is observed with our data, which complement the dataset up to 2 GPa. The dashed orange and red lines materialize the expected water contents of the melts during the HDAC runs at 920 and 950 °C, respectively, given the observed water versus pressure relationship in this figure. A fit (dashed grey line) was performed for easy interpolation. If not visible, errors bar are smaller than symbol size.

termined the water solution as a function of pressure at 1200 °C, and as a function of temperature at 1.0 GPa. The three measurements made at 1.0, 1.5 and 2.0 GPa and 1200 °C are plotted together with the data of McMillan et al. [1986] (Figure 10B). The present data confirm the well-known effect of pressure on water solubility [Burnham and Jahns, 1962, Burnham, 1975, McMillan et al., 1986, McMillan and Holloway, 1987, Mysen and Acton, 1999, Bouyer et al., 2010]. Temperature has a much smaller effect, difficult to detect within the errors of Raman measurements. Changing T from 1000 to 1200 °C results in no visible change in water solubility at 1 GPa (Table 3).

3.6. 700–1300 cm^{-1} portion of Raman spectra from melts in HDAC experiments

From the experiments performed in HDAC cells, previously reported in Le Losq et al. [2017], crystal-free Raman signals of the melt were obtained at ~1.4 GPa and two different temperature conditions: 920 °C and 950 °C. At other conditions [see Table 2 in Le Losq et al., 2017], the 700–1300 cm^{-1} portion of the Raman spectra are mixtures of signals from melts and crystals, such that no quantitative information can be extracted from such spectra.

From melts at 920 °C and 950 °C and ~1.4 GPa, in addition to the O–H stretching signals reported in Le Losq et al. [2017], Raman spectra were also acquired in the 400–1300 cm^{-1} frequency range. Figure 11 shows the spectra corrected from temperature and excitation line effects (see Methods). Neglecting the effect of temperature on water solubility as it appears limited (see Table 3 and Section 3.5), Figure 10B allows estimating that the melts had ~13.4–13.6 wt% dissolved water. For comparison, a spectrum of a glass with 13.6 wt% dissolved water (from one of the solubility experiment) is also reported in Figure 11.

Spectra of the melts present similar features compared to those of glasses, but the intensity of the bands are very different, as well as their width as expected from thermal broadening effects. Compared to a glass with a similar water concentration, we observe that (Figure 11):

- the main band near 500 cm^{-1} is now a shoulder on the left side of the 575 cm^{-1} band, which was assigned to T–O–T vibrations involving Q^2 units;
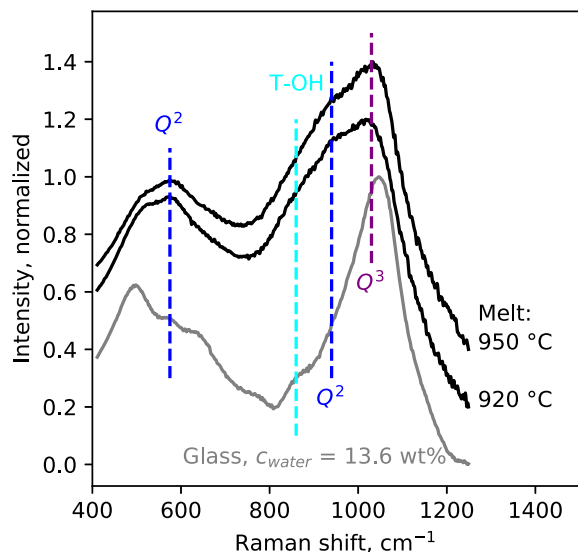
Figure 11. 400–1200 cm^{-1} portion of the unpolarized Raman spectra of the melts at 920 and 950 °C. Pressure at those temperature was of ~1.4 GPa. For comparison, the unpolarized Raman spectrum of a glass with ~13.6 wt% is shown; this glass was obtained during the solubility experiments.

- accordingly, a large increase in intensity is observed at 940 cm^{-1}, at the frequency assigned to T–O stretching in Q^2 units;
- the 860 cm^{-1} shoulder is not clearly visible, but it is clear that there is important contributions at this frequency in the melt spectra;
- the shoulders near 650 and 780 cm^{-1} are not visible in the spectra of the melt;
- the maximum intensity of the 800–1300 cm^{-1} envelop shifts to slightly lower frequency.

Measuring I^{VV}_{860} in the reduced Raman spectra and using $RCS^{VV}_{(Si,Al)-OH}$, OH contents are equal to 11.9±0.7 and 10.6 ± 0.7 wt% at 920 and 950 °C, respectively. Within error bars, they can be considered as comparable, as expected from the small temperature difference. This means that most of the water is dissolved as hydroxyl groups in the melts, while in the glass with the same water content (synthesized at 1.0 GPa and 1200 °C), most of the water is dissolved as H_2O_{mol}. As a result, there is a strong difference in the aluminosilicate structure of the glass and melt. This

is particularly visible when looking at the Raman signal of Q^2 units, significantly smaller in Raman spectra of glasses than in those of melts (Figure 11).

4. Discussion

4.1. *Raman versus infrared water speciation*

Previous attempts to retrieve water speciation in glasses from peak-fitting of the O–H stretching band were done but led to inconclusive results [e.g. Chabiron et al., 2004, Behrens et al., 2006]. A recent study from Helo et al. [2020] also propose to perform a linear decomposition of the O–H stretching band for rhyolite glasses, to retrieve the OH and H_2O_{mol} speciation. The use of the O–H stretching band to retrieve water speciation, from peak fitting or linear decomposition, presents a main problem: this idea starts from the assumption that H_2O_{mol} and OH groups have distinct O–H stretching signals. Data indicate that this assumption can be challenged. First, the O–H stretching signal is strongly affected by hydrogen bonding, which can change significantly as a function of temperature [Walrafen et al., 1986, Frantz et al., 1993, Holtz et al., 1996] as well as glass composition [e.g., Mysen and Virgo, 1986a, Le Losq et al., 2015a]. Then, a principal component analysis of the OH stretching band from the present CAS glass Raman spectra reveals that one component explain 99.5% of the variance of the data. 99.9% of the variance is explained by two components. This indicates that the O–H stretching signals from OH groups and H_2O_{mol} species are quite similar. Small differences may exist, as shown by the partial O–H stretching signals determined by Helo et al. [2020]. However, planning on using those differences to retrieve water speciation is challenging, as shown by the variable success of previous studies. Furthermore, the use of the Raman O–H stretching band requires a calibration against previously measured OH and H_2O_{mol} species concentrations, through infrared spectroscopy for instance. As such, methods based on the use of the Raman O–H stretching band are relative methods. Contrary to this, the approach presented in this study is an absolute method, based on the calculation of apparent Raman cross sections for signals assigned to H_2O_{mol} and T–OH groups. The present approach thus offers another way to determine water speciation, independently of infrared

data. As such, this is an important step as it will allow comparing water speciation data obtained from different ways. However, one potential problem will occur for glasses rich in M–OH species. Indeed, the band near 860 cm^{-1} is assigned to T–OH vibrations. Accordingly, its frequency varies with the glass Si/Al ratio [Malfait, 2009b]. Therefore, this band does not appear to record contributions from M–OH groups. As a consequence, the present method may not work for glasses containing a significant fraction of M–OH groups, like for example the diopside or lithium trisilicate compositions [Xue and Kanzaki, 2008, Le Losq et al., 2015c].

The comparison of water speciation values from FTIR and Raman spectroscopy corroborates the good precision of the present Raman determinations (Figure 6). Raman-determined OH and H_2O_{mol} concentrations compare well with infrared-determined values, except above ~5 wt% water where the Raman method systematically yields higher OH contents (Figure 6). The discrepancy above ~5–6 wt% water can be assigned to (hypothesis 1) the different errors affecting the Raman and IR methods, or (hypothesis 2) to a point where IR spectroscopy begins to fail. Hypothesis 1 is difficult to reconcile with the fact that IR and Raman data agree very well for glasses containing moderate to low water concentrations. Why errors affecting both methods would systematically bias the values they return after a given water concentration?

Hypothesis 2 is more plausible for several reasons. As a starting point, ^{1}H NMR data do not always support the water speciation retrieved from IR spectroscopy for aluminosilicate glasses, as discussed by Cody et al. [2020]. It actually appears that there can be significant discrepancies between both methods. Studying hydrous albite ($NaAlSi_3O_8$) glasses, Cody et al. [2020] reviewed and rejected multiple possible sources of errors and misinterpretation of ^{1}H NMR data. From this, they conclude that ^{1}H NMR data are robust, this leading to the conclusion that the use of 4500 and 5200 cm^{-1} IR bands to retrieve water speciation in such aluminosilicate glasses may actually fail. Now, such failure is not necessarily surprising because the 4500 cm^{-1} IR band used to determine the concentration of OH groups in glasses can be complex. For instance, Le Losq et al. [2015b] reported that the 4500 cm^{-1} IR band becomes unresolved in potassium silicate glasses, because of a broad O–H

stretching signal that extends down to 2000 cm^{-1}, which, therefore, would shift the presumed combination band at 4500 cm^{-1} to frequencies underneath the 3600 cm^{-1} envelope. As the 4500 cm^{-1} is a combination mode of the signal from T–OH groups near 900 cm^{-1} and the O–H stretching signal near 3600 cm^{-1}, any broadening in those signals can affect the resolution of the 4500 cm^{-1} peak. This is reinforced by the overlapping of the 4500 cm^{-1} band with a contribution near 4000 cm^{-1}, which remains not clearly assigned but depends on the total water content in the glass [see review in Cody et al., 2020]. In the case of the present CAS glasses, the 4000 and 4500 cm^{-1} signals overlap at water contents higher than ~5–6 wt%. In Figure 12, we clearly observe this when looking at the infrared spectra of four glasses with nominal water contents ranging from 2 to 8 wt%. The 4500 cm^{-1} band is well resolved in the glasses with 2 and 4 wt% water (Figure 12). However, in glasses containing 6 and 8 wt% water, it is not clearly separated from the 4000 cm^{-1} IR band because the latter and probably the tail of the broad and very intense 3600 cm^{-1} IR O–H stretching signal both contribute some signal near 4300 cm^{-1}. As a result, this probably explains why IR spectroscopy tends to underestimate the concentration of OH groups at water content higher than 5 wt% in the present case (Figure 6). Therefore, at high water content, values for the speciation of water determined from Raman spectra probably are more robust than those estimated from IR data because they rely on the use of the ~860 cm^{-1} Raman band assigned to T–OH vibrations, which shape and frequency are not affected by increasing total water content (Figure 7). This result participates in building the hypothesis than OH concentrations determined through IR spectroscopy may be underestimated in the case of water-rich glasses. This finding is not identical but still in agreement with findings of Cody et al. [2020] for fully polymerized albite glasses. Those authors concluded, from ^{1}H NMR spectroscopy, that IR spectroscopy for albite hydrous glasses was (i) overestimating the concentration of OH groups below ~5 wt% H_2O and (ii) underestimating it above ~5 wt% H_2O. This suggests that the true water speciation in glasses may depend on their composition in a way more complex than previously envisioned.
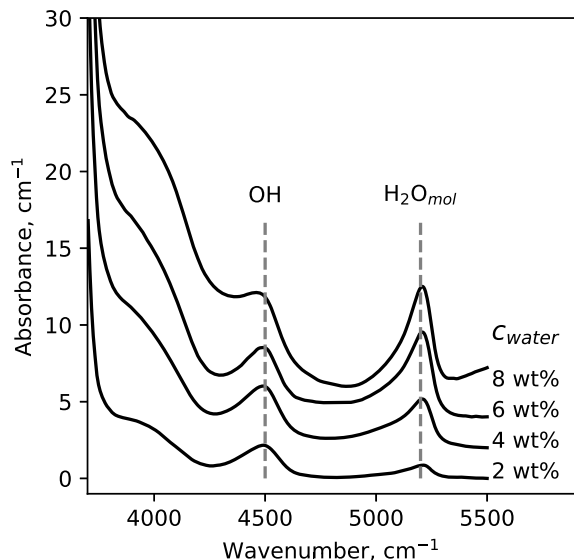
Figure 12. 3800–5500 cm^{-1} portion of IR spectra of four different hydrous CAS glasses, with 2 to 8 wt% dissolved water. The bands near 4500 and 5200 cm^{-1} are assigned to vibrational combination modes of OH groups and H_2O_{mol} species, respectively (see text). The band near 3900 cm^{-1} broadens with increasing the glass water content, so that the limit between this band and the 4500 cm^{-1} signal becomes difficult to distinguish at water contents above 5–6 wt%. This may explain why IR spectroscopy underestimates the OH contents of the glasses above a total water content of 5 wt%, in comparison to Raman spectroscopy (Figure 6).

4.2. *Water effect on glass polymerization*

In the present Ca aluminosilicate glasses, the structural modifications resulting from the addition of water in the glass remains limited (Figures 8, 9). This is not the first time that such limited changes in ^{29}Si NMR or Raman spectra are reported for aluminosilicate compositions. Kohn et al. [1989, 1992, 1998] reported only limited changes in the polymerization of sodium aluminosilicate glasses upon hydration, leading those authors to propose a mechanism of protonation of T–O–T bridges instead of depolymerization. However, recent multinuclear NMR data point to depolymerization rather than protonation [Malfait and Xue, 2010, 2014]. Furthermore, the lack of changes in the Raman and ^{29}Si NMR spectra

cannot be assigned to a compensation of the depolymerization mechanism accompanying formation of T–OH groups by the joint formation of Ca–OH groups [e.g., see Moretti et al., 2014], because in our compositional domain the fraction of Ca–OH groups should be very limited as discussed in Section 3.2. Therefore, it is difficult to reconcile the lack of changes in the Raman and ^{29}Si NMR spectra with the still important fraction of T–OH groups that appear to be present in the glass (Figure 8b). This problem affects our data but also previous studies. For instance, Raman spectra of hydrous silica glass with 5 wt% water display the absence of a ~1100 cm^{-1} Q^3 Raman signal despite the clear presence of an Si–OH signal [Mysen and Virgo, 1986a]. It thus appears that further analysis are necessary to find the origin of this discrepancy.

4.3. *Melt versus glass*

The problem discussed in Section 4.2 may not be extremely important if we actually are interested in melts rather than glasses. Indeed, the HDAC data (Figure 11) show clear and important changes in the Raman spectra, supporting depolymerization of the melt. Results shown in Figure 11 thus indicate that the data from the observation of glasses are not appropriate for making inferences about the effect of water on melt polymerization. First, for anhydrous compositions, small differences already exists between the Raman spectra of glasses and melts. They translate a shift of the equilibria $2Q^n = Q^{n-1} + Q^{n+1}$ to the right-hand side as temperature is increased [Mysen and Frantz, 1993, 1994, Mysen, 1995, 1996, 1999, Kalampounias et al., 2006, Bechgaard et al., 2017]. The large differences observed in this study (Figure 11) may partly arise from such effect, but principally originate from the strong effect of temperature on water speciation [e.g., Nowak and Behrens, 1995, Sowerby and Keppler, 1999, Behrens and Yamashita, 2008, Yamashita et al., 2008, Le Losq et al., 2013, Chertkova and Yamashita, 2015]: increasing T favors the reaction of H_2O_{mol} with T–O–T bonds and the formation of OH groups, leading to the disruption of $Q^3 - Q^4$ units and the formation of depolymerized Q^2 units (Figure 11).

This has important geochemical implications: water speciation data from glasses cannot be used to make inference about processes occurring in melts at

high temperature, and vice-versa. Similarly, observations of the effect of water on the structure of glasses, which actually appear to be affected by some unknown bias, cannot directly be used to make inference about the polymerization of hydrous melts, an important parameter that controls melt mobility and thermodynamic properties, the diffusion of volatile elements including water and CO_2, and even mineral partition coefficients. For instance, for the calculation of water diffusion toward bubbles in magmatic mushes in fluid dynamic models [Gonnermann and Manga, 2007, 2013], it should be necessary to consider the effect of temperature on water speciation and its consequence on melt polymerization. Without such consideration, results will be affected by important bias because the diffusivities of H_2O_{mol} and OH groups are different [see Zhang et al., 2010, and references therein].

5. Conclusion

This study extends our knowledge on the solution mechanisms of water in calc-alkaline melts. Polarized Raman spectroscopy data on the glasses allowed retrieving water speciation in the glasses through a new, absolute method. It is now possible to use the intensity of the Raman peaks at ~860–900 cm^{-1} and 1630 cm^{-1} to retrieve the concentration of T–OH and H_2O_{mol} species in hydrous glasses. We applied the method to the present CAS glass composition with a very good success. Results compares very well with the IR-determined values, except at high water contents where IR results appeared biased. Indeed, above ~5 wt% dissolved water, the OH content retrieved from IR spectra appears underestimated due to a broadening and decrease in resolution of the 4500 cm^{-1} IR band that may influence the determination in OH group concentration. This corroborates previous results from ^{1}H NMR spectroscopy on albite glass compositions [Cody et al., 2020].

The analysis of the silicate signals in the Raman spectra as well as of the ^{29}Si MAS NMR of the hydrous CAS glasses reveal limited changes with water addition in the Raman bands assigned to vibrations in Q^n tetrahedral units. However, from melt Raman spectra, it also is found that melt polymerization differs strongly from that of a glass with a similar content as shown by Raman spectra (Figure 11), due to much

higher OH contents. Such differences should be considered, for instance in models of water diffusion in magmas.

Conflicts of interest

Authors have no conflicts of interest to declare.

Acknowledgements

References

Balzer, R., Behrens, H., Waurischk, T., Reinsch, S., Müller, R., Kiefer, P., Deubener, J., and Fechtelkord, M. (2020). Water in alkali aluminosilicate glasses. *Front. Mater.*, 7, 1–17.

Bancroft, G. M., Nesbitt, H. W., Henderson, G. S., O'Shaughnessy, C., Withers, A. C., and Neuville, D. R. (2018). Lorentzian dominated lineshapes and linewidths for Raman symmetric stretch peaks (800–1200 cm^{-1}) in Q^n ($n = 1$–3) species of alkali silicate glasses/melts. *J. Non-Cryst. Solids*, 484, 72–83.

Bassett, W. A., Anderson, A. J., Mayanovic, R. A., and Chou, I.-M. (2000). Hydrothermal diamond anvil cell for XAFS studies of first-row transition elements in aqueous solution up to supercritical conditions. *Chem. Geol.*, 167, 3–10.

Bassett, W. A., Shen, A. H., Bucknum, M., and Chou, I. M. (1994). A new diamond cell for hydrothermal studies to 2.5 GPa and from $-190\,°C$ to $1200\,°C$. *Rev. Sci. Instrum.*, 64, 2340–2345.

Bassett, W. A., Wu, T. C., Chou, I. M., Haselton Jr, H. T., Frantz, J., Mysen, B. O., Huang, W. L., Sharma, K., and Schiferl, D. (1996). The hydrothermal diamond anvil cell (HDAC) and its applications. In *Mineral Spectroscopy: A Tribute to Roger G. Burns*, pages 261–272. The Geochemical Society Special Publication, Washington, DC.

Bechgaard, T. K., Scannell, G., Huang, L., Young-man, R. E., Mauro, J. C., and Smedskjaer, M. M. (2017). Structure of MgO/CaO sodium aluminosilicate glasses: Raman spectroscopy study. *J. Non-Cryst. Solids*, 470, 145–151.

Behrens, H., Meyer, M., Holtz, F., Benne, D., and Nowak, M. (2001). The effect of alkali ionic radius, temperature and pressure on the solubility of water in MAlSi$_3$O$_8$ melts (M = Li, Na, K, Rb). *Chem. Geol.*, 174, 275–289.

Behrens, H., Romano, C., Nowak, M., Holtz, F., and Dingwell, D. B. (1996). Near-infrared spectroscopic determination of water species in glasses of the system MAlSi$_3$O$_8$ (M = Li, Na, K): an interlaboratory study. *Chem. Geol.*, 128, 41–63.

Behrens, H., Roux, J., Neuville, D. R., and Siemann, M. (2006). Quantification of dissolved H$_2$O in silicate glasses using confocal microRaman spectroscopy. *Chem. Geol.*, 229, 96–112.

Behrens, H. and Yamashita, S. (2008). Water speciation in hydrous sodium tetrasilicate and hexasilicate melts: Constraint from high temperature NIR spectroscopy. *Chem. Geol.*, 256, 306–315.

Bell, R. J., Bird, N. F., and Dean, P. (1968). The vibrational spectra of vitreous silica, germania and beryllium fluoride. *J. Phys. C (Proc. Phys. Soc.)*, 1, 299–303.

Bohlen, S. R. (1984). Equilibria for precise pressure calibration and a frictionless furnace assembly for the piston–cylinder apparatus. *Neues Jahrb. Mineral.—Monatshefte*, 9, 404–412.

Bouyer, F., Geneste, G., Ispas, S., Kob, W., and Ganster, P. (2010). Water solubility in calcium aluminosilicate glasses investigated by first principles techniques. *J. Solid State Chem.*, 183, 2786–2796.

Boyd, F. R. and England, J. L. (1960). Apparatus for phase-equilibrium measurements at pressures up to 50 Kilobars and temperatures up to 1750 °C. *J. Geophys. Res.*, 65, 741–748.

Brawer, S. A. and White, W. B. (1975). Raman spectroscopic investigation of the structure of silicate glasses. I. The binary alkali silicates. *J. Chem. Phys.*, 63, 2421–2432.

Brawer, S. A. and White, W. B. (1977). Raman spectroscopic investigation of the structure of silicate glasses. II. Soda-alkaline earth-alumina ternary and quaternary glasses. *J. Non-Cryst. Solids*, 23, 261–278.

Bucheneau, U., Prager, M., Nücker, N., Dianoux, A. J., Ahmad, N., and Phillips, W. A. (1986). Low-frequency modes in vitreous silica. *Phys. Rev. B*, 34, 5665–5673.

Burnham, C. W. (1975). Water and magmas; a mixing model. *Geochim. Cosmochim. Acta*, 39, 1077–1084.

Burnham, C. W. and Jahns, R. H. (1962). A method for determining the solubility of water in silicate melts. *Am. J. Sci.*, 260, 721–745.

Campbell, I. H. and Taylor, S. R. (1983). No water, no granites—No oceans, no continents. *Geophys. Res. Lett.*, 10, 1061–1064.

Chabiron, A., Pironon, J., and Massare, D. (2004). Characterization of water in synthetic rhyolitic glasses and natural melt inclusions by Raman spectroscopy. *Contrib. Mineral. Petrol.*, 146, 485–492.

Chertkova, N. and Yamashita, S. (2015). In situ spectroscopic study of water speciation in the depolymerized Na$_2$Si$_2$O$_5$ melt. *Chem. Geol.*, 409, 149–156.

Chumakov, A. I., Monaco, A., Crichton, W. A., Bosak, A., Rüffer, R., Meyer, A., Kargl, F., Comez, L., Fioretto, D., Giefers, H., et al. (2011). Equivalence of the Boson Peak in glasses to the transverse acoustic van Hove singularity in crystals. *Phys. Rev. Lett.*, 106, 1–5, article no. 225501.

Cody, G. D., Ackerson, M., Beaumont, C., Foustoukos, D., Le Losq, C., and Mysen, B. O. (2020). Revisiting water speciation in hydrous alumino-silicate glasses: A discrepancy between solid-state ^{1}H NMR and NIR spectroscopy in the determination of X–OH and H$_2$O. *Geochim. Cosmochim. Acta*, 285, 150–174.

Cody, G. D., Mysen, B. O., and Lee, S. K. (2005). Structure versus composition: A solid-state ^{29}Si NMR study of quenched glasses along the Na$_2$O–SiO$_2$–H$_2$O join. *Geochim. Cosmochim. Acta*, 69, 2373–2384.

Dalou, C., Le Losq, C., and Mysen, B. O. (2015a). In situ study of the fractionation of hydrogen isotopes between aluminosilicate melts and coexisting aqueous fluids at high pressure and high temperature—Implications for the δD in magmatic processes. *Earth Planet. Sci. Lett.*, 426, 158–166.

Dalou, C., Le Losq, C., Mysen, B. O., and Cody, G. D. (2015b). Solubility and solution mechanisms of chlorine and fluorine in aluminosilicate melts at high pressure and high temperature. *Am. Mineral.*, 100, 2272–2283.

Davis, K. M. and Tomozawa, M. (1996). An infrared

spectroscopic study of water-related species in silica glasses. *J. Non-Cryst. Solids*, 201, 177–198.

Deubener, J., Müller, R., Behrens, H., and Heide, G. (2003). Water and the glass transition temperature of silicate melts. *J. Non-Cryst. Solids*, 330, 268–273.

Di Muro, A., Villemant, B., Montagnac, G., Scaillet, B., and Reynard, B. (2006). Quantification of water content and speciation in natural silicic glasses (phonolite, dacite, rhyolite) by confocal microRaman spectrometry. *Geochim. Cosmochim. Acta*, 70, 2868–2884.

Dingwell, D. B., Romano, C., and Hess, K.-U. (1996). The effect of water on the viscosity of a haplogranitic melt under P–T–X conditions relevant to silicic volcanism. *Contrib. Mineral. Petrol.*, 124, 19–28.

Farnan, I., Kohn, S. C., and Dupree, R. (1987). A study of the structural role of water in hydrous silica glass using cross-polarisation magic angle spinning NMR. *Geochim. Cosmochim. Acta*, 51, 2869–2873.

Frantz, J. D., Dubessy, J., and Mysen, B. (1993). An optical cell for Raman spectroscopic studies of supercritical fluids and its application to the study of water to 500 °C and 2000 bar. *Chem. Geol.*, 106, 9–26.

Friedman, I., Long, W., and Smith, R. L. (1963). Viscosity and water content of rhyolite glass. *J. Geophys. Res.*, 68, 6523–6535.

Furukawa, T., Fox, K. E., and White, W. B. (1981). Raman spectroscopic investigation of the structure of silicate glasses. III. Raman intensities and structural units in sodium silicate glasses. *J. Chem. Phys.*, 75, 3226–3237.

Furukawa, T. and White, W. B. (1980). Vibrational spectra and glass structure. *J. Non-Cryst. Solids*, 38, 87–92.

Galeener, F. L. (1979). Band limits and the vibrational spectra of tetrahedral glasses. *Phys. Rev. B*, 19, 4292–4397.

Gonnermann, H. M. (2015). Magma fragmentation. *Annu. Rev. Earth Planet. Sci.*, 43, 431–458.

Gonnermann, H. M. and Manga, M. (2007). The fluid mechanics inside a volcano. *Annu. Rev. Fluid Mech.*, 39, 321–356.

Gonnermann, H. M. and Manga, M. (2013). Dynamics of magma ascent in the volcanic conduit. In Fagents, S. A., Gregg, T. K. P., and Lopes, R. M. C., editors, *Modeling Volcanic Processes: The Physics and Mathematics of Volcanism*, pages 55–84. Cambridge University Press, Cambridge, UK.

Helo, C., Castro, J. M., Hess, K.-U., and Dingwell, D. B. (2020). Determination of water speciation in hydrous haplogranitic glasses with partial Raman spectra. *Chem. Geol.*, 553, article no. 119793.

Herzog, F. and Zakaznova-Herzog, V. P. (2011). Quantitative Raman spectroscopy: Challenges, shortfalls, and solutions—Application to calcium silicate glasses. *Am. Mineral.*, 96, 914–927.

Hoffman, M. D. and Gelman, A. (2014). The no-U-turn sampler: Adaptively setting path lengths in Hamiltonian Monte Carlo. *J. Mach. Learn. Res.*, 15, 1593–1623.

Holtz, F., Bény, J. M., Mysen, B. O., and Pichavant, M. (1996). High-temperature Raman spectroscopy of silicate and aluminosilicate hydrous glasses: Implications for water speciation. *Chem. Geol.*, 128, 25–39.

Kalampounias, A. G., Yannopoulos, S. N., and Papatheodorou, G. N. (2006). A high-temperature Raman spectroscopic investigation of the potassium tetrasilicate in glassy, supercooled, and liquid states. *J. Chem. Phys.*, 125, article no. 164502.

Kohn, S. C., Dupree, R., and Mortuza, M. G. (1992). The interaction between water and aluminosilicate magmas. *Chem. Geol.*, 96, 399–409.

Kohn, S. C., Dupree, R., and Smith, M. E. (1989). A multinuclear magnetic resonance study of the structure of hydrous albite glass. *Geochim. Cosmochim. Acta*, 53, 2925–2935.

Kohn, S. C., Smith, M. E., Dirken, P. J., Van Eck, E. R. H., Kentgens, A. P. M., and Dupree, R. (1998). Sodium environment in dry and hydrous albite glasses: Improved ^{23}Na solid state NMR data and their implications for water dissolution mechanisms. *Geochim. Cosmochim. Acta*, 62, 79–87.

Kushiro, I. (1976). A new furnace assembly with a small temperature gradient in solid-media, high-pressure apparatus. In *Carnegie Institution of Washington Year Book*, volume 75, pages 832–833. Carnegie Institution of Washington, Washington D.C., USA.

Kushiro, I., Syono, Y., and Akimoto, S. (1968a). Melting of a peridotite nodule at high pressures and high water pressures. *J. Geophys. Res.*, 73, 6023–6029.

Kushiro, I., Yoder, H. S., and Nishikawa, M. (1968b). Effect of water on the melting of enstatite. *Geol. Soc. Am. Bull.*, 79, 1685–1692.

Le Losq, C. (2018). Rampy: a Python library for processing spectroscopic (IR, Raman, XAS…) data. https://doi.org/10.5281/zenodo.1168730. Zenodo.

Le Losq, C., Cody, G. D., and Mysen, B. O. (2015a). Alkali influence on the water speciation and the environment of protons in silicate glasses revealed by ^{1}H MAS NMR spectroscopy. *Am. Mineral.*, 100, 466–473.

Le Losq, C., Cody, G. D., and Mysen, B. O. (2015b). Complex IR spectra of OH^- groups in silicate glasses: Implications for the use of the 4500 cm^{-1} IR peak as a marker of OH^- groups concentration. *Am. Mineral.*, 100, 945–950.

Le Losq, C., Dalou, C., and Mysen, B. O. (2017). In situ study at high pressure and temperature of the environment of water in hydrous Na and Ca aluminosilicate melts and coexisting aqueous fluids. *J. Geophys. Res.: Solid Earth*, 122, 4888–4899.

Le Losq, C., Moretti, R., and Neuville, D. R. (2013). Speciation and amphoteric behavior of water in aluminosilicate melts and glasses: High-Temperature Raman spectroscopy and reaction equilibria. *Eur. J. Mineral.*, 25, 777–790.

Le Losq, C., Mysen, B. O., and Cody, G. D. (2015c). Water and magmas: insights about the water solution mechanisms in alkali silicate melts from infrared, Raman, and ^{29}Si solid-state NMR spectroscopies. *Prog. Earth Planet. Sci.*, 2, article no. 22.

Le Losq, C. and Neuville, D. R. (2013). Effect of the Na/K mixing on the structure and the rheology of tectosilicate silica-rich melts. *Chem. Geol.*, 346, 57–71.

Le Losq, C., Neuville, D. R., Florian, P., Henderson, G. S., and Massiot, D. (2014). The role of Al^{3+} on rheology and structural changes of sodium silicate and aluminosilicate glasses and melts. *Geochim. Cosmochim. Acta*, 126, 495–517.

Le Losq, C., Neuville, D. R., Moretti, R., and Roux, J. (2012). Determination of water content in silicate glasses using Raman spectrometry: Implications for the study of explosive volcanism. *Am. Mineral.*, 97, 779–790.

Leonteva, A. (1940). Measurements of the viscosity of obsidian and of hydrated glasses. *Izv. Akad. Nauk SSSR, Ser. Geol.*, 2, 44–54.

Maekawa, H., Maekawa, T., Kawamura, K., and Yokokawa, T. (1991). The structural groups of alkali silicate glasses determined from ^{29}Si MAS-NMR. *J. Non-Cryst. Solids*, 127, 53–64.

Malfait, W. J. (2009a). Quantitative Raman spectroscopy: speciation of cesium silicate glasses. *J. Raman Spectrosc.*, 40, 1895–1901.

Malfait, W. J. (2009b). The 4500 cm^{-1} infrared absorption band in hydrous aluminosilicate glasses is a combination band of the fundamental Si, Al–OH and O–H vibrations. *Am. Mineral.*, 94, 849–852.

Malfait, W. J. (2014). The nearly complete dissociation of water in glasses with strong aluminum avoidance. *Am. Mineral.*, 99, 1648–1652.

Malfait, W. J., Seifert, R., Petitgirard, S., Mezouar, M., and Sanchez-Valle, C. (2014a). The density of andesitic melts and the compressibility of dissolved water in silicate melts at crustal and upper mantle conditions. *Earth Planet. Sci. Lett.*, 393, 31–38.

Malfait, W. J., Seifert, R., Petitgirard, S., Perrillat, J.-P., Mezouar, M., Ota, T., Nakamura, E., Lerch, P., and Sanchez-Valle, C. (2014b). Supervolcano eruptions driven by melt buoyancy in large silicic magma chambers. *Nat. Geosci.*, 7, 122–125.

Malfait, W. J. and Xue, X. (2010). The nature of hydroxyl groups in aluminosilicate glasses: Quantifying Si–OH and Al–OH abundances along the SiO_2–$NaAlSiO_4$ join by ^{1}H, ^{27}Al–^{1}H and ^{29}Si–^{1}H NMR spectroscopy. *Geochim. Cosmochim. Acta*, 74, 719–737.

Malfait, W. J. and Xue, X. (2014). Hydroxyl speciation in felsic magmas. *Geochim. Cosmochim. Acta*, 140, 606–620.

Malinovsky, V. K. and Sokolov, A. P. (1986). The nature of boson peak in Raman scattering in glasses. *Solid State Commun.*, 57, 757–761.

Mao, H. K., Bell, P. M., and England, J. L. (1971). Tensional errors and drift of the thermocouple electromotive force in the single stage, piston–cylinder apparatus. In *Carnegie Institution of Washington Year Book*, volume 70, pages 281–287. Carnegie Institution of Washington, Washington D.C., USA.

Matson, D. W., Sharma, S. K., and Philpotts, J. A. (1983). The structure of high-silica alkali-silicate glasses. A Raman spectroscopic investigation. *J. Non-Cryst. Solids*, 58, 323–352.

McMillan, P., Peraudeau, G., Holloway, J., and Coutures, J.-P. (1986). Water solubility in a calcium aluminosilicate melt. *Contrib. Mineral. Petrol.*, 94, 178–182.

McMillan, P. and Remmele Jr, R. L. (1986). Hydroxyl-

sites in SiO_2 glass: A note on infrared and Raman spectra. *Am. Mineral.*, 71, 772–778.

McMillan, P. F. (1984). Structural studies of silicate glasses and melts—Applications and limitations of Raman spectroscopy. *Am. Mineral.*, 69, 622–644.

McMillan, P. F. and Holloway, J. R. (1987). Water solubility in aluminosilicate melts. *Contrib. Mineral. Petrol.*, 97, 320–332.

Moretti, R., Le Losq, C., and Neuville, D. R. (2014). The amphoteric behavior of water in silicate melts from the point of view of their ionic-polymeric constitution. *Chem. Geol.*, 367, 23–33.

Mysen, B. (2010). Structure of H_2O-saturated peralkaline aluminosilicate melt and coexisting aluminosilicate-saturated aqueous fluid determined in-situ to 800 °C and ~800 MPa. *Geochim. Cosmochim. Acta*, 74, 4123–4139.

Mysen, B. O. (1990). Role of Al in depolymerized, peralkaline aluminosilicate melts in the systems Li_2O–Al_2O_3–SiO_2, Na_2O–Al_2O_3–SiO_2, and K_2O–Al_2O_3–SiO_2. *Am. Mineral.*, 75, 120–134.

Mysen, B. O. (1995). Experimental, in situ, high-temperature studies of properties and structure of silicate melts relevant to magmatic processes. *Eur. J. Mineral.*, 7, 745–766.

Mysen, B. O. (1996). Haploandesitic melts at magmatic temperatures: In situ, high-temperature structure and properties of melts along the join $K_2Si_4O_9$–$K_2(KAl)_4O_9$ to 1236 °C at atmospheric pressure. *Geochim. Cosmochim. Acta*, 60, 3665–3685.

Mysen, B. O. (1999). Structure and properties of magmatic liquids: From haplobasalt to haploandesite. *Geochim. Cosmochim. Acta*, 63, 95–112.

Mysen, B. O. (2009). Solution mechanisms of silicate in aqueous fluid and H_2O in coexisting silicate melts determined in-situ at high pressure and high temperature. *Geochim. Cosmochim. Acta*, 73, 5748–5763.

Mysen, B. O. (2014). Water-melt interaction in hydrous magmatic systems at high temperature and pressure. *Prog. Earth Planet. Sci.*, 1, 1–18.

Mysen, B. O. and Acton, M. (1999). Water in H_2O-saturated magma–fluid systems: solubility behavior in K_2O–Al_2O_3–SiO_2–H_2O to 2.0 GPa and 1300 °C. *Geochim. Cosmochim. Acta*, 63, 3799–3815.

Mysen, B. O. and Cody, G. D. (2005). Solution mechanisms of H_2O in depolymerized peralkaline melts. *Geochim. Cosmochim. Acta*, 69, 5557–5566.

Mysen, B. O., Finger, L. W., Virgo, D., and Seifert, F. A. (1982). Curve-fitting of Raman spectra of silicate glasses. *Am. Mineral.*, 67, 686–695.

Mysen, B. O. and Frantz, J. D. (1993). Structure of silicate melts at high temperature: In-situ measurements in the system BaO–SiO_2. *Am. Mineral.*, 78, 699–709.

Mysen, B. O. and Frantz, J. D. (1994). Silicate melts at magmatic temperatures: in-situ structure determination to 1651 °C and effect of temperature and bulk composition on the mixing behavior of structural units. *Contrib. Mineral. Petrol.*, 117, 1–14.

Mysen, B. O., Lucier, A., and Cody, G. D. (2003). The structural behavior of Al^{3+} in peralkaline melts and glasses in the system Na_2O–Al_2O_3–SiO_2. *Am. Mineral.*, 88, 1668–1678.

Mysen, B. O. and Toplis, M. J. (2007). Structural behavior of Al^{3+} in peralkaline, metaluminous, and peraluminous silicate melts and glasses at ambient pressure. *Am. Mineral.*, 92, 933–946.

Mysen, B. O. and Virgo, D. (1986a). Volatiles in silicate melts at high pressure and temperature 1. Interaction between OH groups and Si^{4+}, Al^{3+}, Ca^{2+}, Na^+ and H^+. *Chem. Geol.*, 57, 303–331.

Mysen, B. O. and Virgo, D. (1986b). Volatiles in silicate melts at high pressure and temperature 2. Water in melts alon the join $NaAlO_2$–SiO_2 and a comparison of solubility mechanisms of water and fluorine. *Chem. Geol.*, 57, 333–358.

Mysen, B. O. and Wheeler, K. (2000). Solubility behavior of water in haploandesitic melts at high pressure and high temperature. *Am. Mineral.*, 85, 1128–1142.

Mysen, B. O. and Yamashita, S. (2010). Speciation of reduced C–O–H volatiles in coexisting fluids and silicate melts determined in-situ to ~1.4 GPa and 800 °C. *Geochim. Cosmochim. Acta*, 74, 4577–4588.

Nakamura, K., Takahashi, Y., Osada, M., and Fujiwara, T. (2013). Low-frequency Raman scattering in binary silicate glass: Boson peak frequency and its general expression. *J. Ceramic Soc. Japan*, 121, 1012–1014.

Neal, R. M. (2011). MCMC using Hamiltonian dynamics. In *Handbook of Markov Chain Monte Carlo*, pages 113–162. Chapman and Hall/CRC, New York.

Nesbitt, H. W., O'Shaughnessy, C., Henderson, G. S., Michael Bancroft, G., and Neuville, D. R. (2019). Factors affecting line shapes and intensities of Q^3

and Q^4 Raman bands of Cs silicate glasses. *Chem. Geol.*, 505, 1–11.

Neuville, D. R. (2006). Viscosity, structure and mixing in (Ca, Na) silicate melts. *Chem. Geol.*, 229, 28–41.

Neuville, D. R., Cormier, L., and Massiot, D. (2004). Al environment in tectosilicate and peraluminous glasses: A ^{27}Al MQ-MAS NMR, Raman, and XANES investigation. *Geochim. Cosmochim. Acta*, 68, 5071–5079.

Neuville, D. R., Cormier, L., and Massiot, D. (2006). Al coordination and speciation in calcium aluminosilicate glasses: Effects of composition determined by ^{27}Al MQ-MAS NMR and Raman spectroscopy. *Chem. Geol.*, 229, 173–185.

Neuville, D. R., Cormier, L., Montouillout, V., Florian, P., Millot, F., Rifflet, J. C., and Massiot, D. (2008). Structure of Mg and Mg/Ca aluminosilicate glasses: ^{27}Al NMR and Raman spectroscopy investigations. *Am. Mineral.*, 83, 1721–1731.

Neuville, D. R. and Mysen, B. O. (1996). Role of aluminium in the silicate network: In situ, high-temperature study of glasses and melts on the join SiO_2–$NaAlO_2$. *Geochim. Cosmochim. Acta*, 60, 1727–1737.

Novikov, A. N., Neuville, D. R., Hennet, L., Gueguen, Y., Thiaudière, D., Charpentier, T., and Florian, P. (2017). Al and Sr environment in tectosilicate glasses and melts: Viscosity, Raman and NMR investigation. *Chem. Geol.*, 461, 115–127.

Nowak, M. and Behrens, H. (1995). The speciation of water in haplogranitic glasses and melts determined by in situ near-infrared spectroscopy. *Geochim. Cosmochim. Acta*, 59, 3445–3450.

Ochs, F. A. and Lange, R. A. (1999). The density of hydrous magmatic liquids. *Science*, 283, 1314–1317.

Richet, P., Lejeune, A.-M., Holtz, F., and Roux, J. (1996). Water and the viscosity of andesite melts. *Chem. Geol.*, 128, 185–197.

Richet, P., Whittington, A., Holtz, F., Behrens, H., Ohlhorst, S., and Wilke, M. (2000). Water and the density of silicate glasses. *Contrib. Mineral. Petrol.*, 138, 337–347.

Salvatier, J., Wiecki, T. V., and Fonnesbeck, C. (2016). Probabilistic programming in Python using PyMC3. *PeerJ Comput. Sci.*, 2, article no. e55.

Saucier, H. (1952). Quelques expériences sur la viscosité à haute température de verres ayant la composition d'un granite. Influence de la vapeur d'eau sous pression. *Bull. Soc. Fr. Minéral. Cristal.*, 75, 1–

45.

Schiavi, F., Bolfan-Casanova, N., Withers, A. C., Médard, E., Laumonier, M., Laporte, D., Flaherty, T., and Gómez-Ulla, A. (2018). Water quantification in silicate glasses by Raman spectroscopy: Correcting for the effects of confocality, density and ferric iron. *Chem. Geol.*, 483, 312–331.

Seifert, F., Mysen, B. O., and Virgo, D. (1982). Three-dimensional network structure of quenched melts (glass) in the systems SiO_2–$NaAlO_2$, SiO_2–$CaAl_2O_4$ and SiO_2–$MgAl_2O_4$. *Am. Mineral.*, 67, 696–717.

Sen, P. N. and Thorpe, M. F. (1977). Phonons in AX_2 glasses: From molecular to band-like modes. *Phys. Rev. B*, 15, 4030–4038.

Shintani, H. and Tanaka, H. (2008). Universal link between the boson peak and transverse phonons in glass. *Nat. Mater.*, 7, 870–877.

Silver, L. A., Ihinger, P. D., and Stolper, E. (1990). The influence of bulk composition on the speciation of water in silicate glasses. *Contrib. Mineral. Petrol.*, 104, 142–162.

Sowerby, J. R. and Keppler, H. (1999). Water speciation in rhyolitic melt determined by in-situ infrared spectroscopy. *Am. Mineral.*, 84, 1843–1849.

Spiekermann, G., Steele-MacInnis, M., Kowalski, P. M., Schmidt, C., and Jahn, S. (2013). Vibrational properties of silica species in MgO–SiO_2 glasses obtained from ab initio molecular dynamics. *Chem. Geol.*, 346, 22–33.

Spiekermann, G., Steele-MacInnis, M., Schmidt, C., and Jahn, S. (2012). Vibrational mode frequencies of silica species in SiO_2–H_2O liquids and glasses from ab initio molecular dynamics. *J. Chem. Phys.*, 136, article no. 154501.

Stolen, R. H. and Walrafen, G. E. (1976). Water and its relation to broken bond defects in fused silica. *J. Chem. Phys.*, 64, 2623–2631.

Stolper, A. (1982). Water in silicate glasses: An infrared spectroscopic study. *Contrib. Mineral. Petrol.*, 81, 1–17.

Thomas, R. (2000). Determination of water contents of granite melt inclusions by confocal laser Raman microprobe spectroscopy. *Am. Mineral.*, 85, 868–872.

Walrafen, G. E. (1964). Raman spectral studies of water structure. *J. Chem. Phys.*, 40, 3249–3256.

Walrafen, G. E. (1975). Raman spectra from Si–OH groups in solid optical fibers. *J. Chem. Phys.*, 62, 297–298.

Walrafen, G. E., Fisher, M. R., Hokmabadi, M. S., and Yang, W.-H. (1986). Temperature dependence of the low- and high-frequency Raman scattering from liquid water. *J. Chem. Phys.*, 85, 6970–6982.

Walrafen, G. E. and Samantha, S. R. (1978). Infrared absorbance spectra and interactions involving OH groups in fused silica. *J. Chem. Phys.*, 69, 493–495.

Xue, X. (2009). Water speciation in hydrous silicate and aluminosilicate glasses: Direct evidence from ^{29}Si–^{27}Al–^{1}H double-resonance NMR. *Am. Mineral.*, 94, 395–398.

Xue, X. and Kanzaki, M. (2004). Dissolution mechanisms of water in depolymerized silicate melts: Constraints from ^{29}Si NMR spectroscopy and ab initio calculations. *Geochim. Cosmochim. Acta*, 68, 5027–5057.

Xue, X. and Kanzaki, M. (2006). Depolymerization effect of water in aluminosilicate glasses: Direct evidence from ^{27}Al heteronuclear correlation NMR. *Am. Mineral.*, 91, 1922–1926.

Xue, X. and Kanzaki, M. (2008). Structure of hydrous aluminosilicate glasses along the diopside–anorthite join: A comprehensive one- and two-dimensional ^{1}H and ^{27}Al NMR study. *Geochim. Cosmochim. Acta*, 72, 2331–2348.

Yamashita, S., Behrens, H., Schmidt, B. C., and Dupree, R. (2008). Water speciation in sodium silicate glasses based on NIR and NMR spectroscopy. *Chem. Geol.*, 256, 231–241.

You, J.-L., Jiang, G.-C., Hou, H.-Y., Chen, H., Wu, Y.-Q., and Xu, K.-D. (2005). Quantum chemistry study on superstructure and Raman spectra of binary sodium silicates. *J. Raman Spectrosc.*, 36, 237–249.

Zajacz, Z., Halter, W., Malfait, W. J., Bachmann, O., Bodnar, R. J., Hirschmann, M. M., Mandeville, C. W., Morizet, Y., Müntener, O., Ulmer, P., et al. (2005). A composition-independent quantitative determination of the water content in silicate glasses and silicate melt inclusions by confocal Raman spectroscopy. *Contrib. Mineral. Petrol.*, 150, 631–642.

Zakaznova-Herzog, V. P, Malfait, W. J., Herzog, F., and Halter, W. E. (2007). Quantitative Raman spectroscopy: Principles and application to potassium silicate glasses. *J. Non-Cryst. Solids*, 353, 4015–4028.

Zhang, Y., Ni, H., and Chen, Y. (2010). Diffusion data in silicate melts. *Rev. Mineral. Geochem.*, 72, 311–408.

Zotov, N., Delaplane, R. G., and Keppler, H. (1998). Structural changes in sodium tetrasilicate glass around the liquid-glass transition: a neutron diffraction study. *Phys. Chem. Minerals*, 26, 107–110.

Zotov, N., Ebbsjö, I., Timpel, D., and Keppler, H. (1999). Calculation of Raman spectra and vibrational properties of silicate glasses: comparison between $Na_2Si_4O_9$ and SiO_2 glasses. *Phys. Rev. B*, 60, 6383–6397.